Solid Oxide Fuel Cells Modeling

Domenico Ferrero, Andrea Lanzini and Massimo Santarelli

Abstract A solid oxide fuel cell (SOFC) is a complex system consisting of different components, in which interconnected physical phenomena occur simultaneously and contribute to determine the global thermo-electrochemical response of the system. The simulation and prediction of the response of an SOFC are of paramount importance for the analysis of possible applications without resorting to extensive experimental investigations. Simulating the SOFC response requires to develop reliable models that can describe the significant phenomena occurring in the system. Different approaches can be followed for the SOFC modeling, depending on the goals of the model. This chapter will provide an introduction to SOFC modeling focusing on a macroscopic, physically based approach.

Abbreviations

List of Symbols

a	Thermodynamic activity
B_p	Permeability (m^2)
C_f	Drag constant
C_p	Specific heat at constant pressure (J kg^{-1} K^{-1})
d	Molecule, particle, pore diameter (m, μm)
D	Diffusion coefficient (m^2 s^{-1}, cm^2 s^{-1})
D_T	Thermal diffusion coefficient (kg m^{-1} s^{-1})
E	Equilibrium, electrode potential (V)
E_{act}	Activation energy (J mol^{-1})
E_b	Emissive power of black body (W m^{-2})
f	Volume fraction of ionic/electronic phase in the electrode
$\boldsymbol{f}$	Body forces acting on the fluid (m s^{-2})
F	Faraday's constant (C mol^{-1})
$\boldsymbol{F}$	Volume force (N m^{-3})
F_{i-j}	View factor between i and j surface elements

D. Ferrero · A. Lanzini · M. Santarelli (✉)
Energy Department, Polytechnic of Turin, Turin, Italy
e-mail: massimo.santarelli@polito.it

M. Boaro and A.S. Aricò (eds.), *Advances in Medium and High Temperature Solid Oxide Fuel Cell Technology*, CISM International Centre for Mechanical Sciences 574,
DOI 10.1007/978-3-319-46146-5_8

$\bar{g}$ Molar Gibbs free energy variation (J mol^{-1})
$\bar{h}$ Molar enthalpy (J mol^{-1})
H_0 Incident irradiation (W m^{-2})
i Current density (A m^{-2})
i_0 Exchange current density (A m^{-2})
i_v Volumetric current density (A m^{-3})
i_{TPB} Current per unit of TPB length (A m^{-1})
I Current (A)
$\vec{j}$ Mass flux (kg m^{-2} s^{-1})
k Thermal conductivity (W m^{-1} K^{-1})
k_B Boltzmann constant (J K^{-1})
K_r Equilibrium constant of r reaction
L_p Characteristic size of the pore (m)
M_n Molecular weight (kg mol^{-1})
n Number of electrons involved in redox reactions
p Pressure (Pa, bar)
P Percolation probability
q Rate of charge-transfer reaction (mol m^{-1} s^{-1})
$\vec{q}$ Heat flux (W m^{-2})
Q Volumetric heat source (W m^{-3})
r Reaction rate (mol m^{-3} s^{-1})
R Ideal gas constant (J mol^{-1} K^{-1})
R_{con} Contact resistance (Ω cm^2)
$\bar{s}$ Molar entropy (J mol^{-1} K^{-1})
$\dot{s}_k$ Molar rate of k species (mol cm^{-2} s^{-1})
S Mass source term (kg m^{-3} s^{-1})
t Time (s)
T Temperature (K)
$\boldsymbol{u}$ Fluid velocity vector (m s^{-1})
$\bar{\boldsymbol{u}}$ Superficial velocity (m s^{-1})
V Cell voltage (V)
V_a Atomic diffusion volumes (cm^3 mol^{-1})
x Mass fraction
$[X]$ Molar concentration (mol m^{-3}, mol m^{-2})
y Molar fraction

Greek Symbols

α Symmetry coefficient of Butler–Volmer equation
β Symmetry coefficient of charge-transfer reaction
β_e Extinction coefficient of the medium (m^{-1})
γ Pre-exponential activation parameter (A cm^{-2})
γ_s Scaling factor (1 or m^{-1})
γ_{0i} Sticking coefficient of i-reaction

Γ	Surface site density (mol cm^{-2})
ε	Porosity
η	Overpotential (V)
θ_k	Surface coverage of k species
λ	Mean free path (m)
λ_{TPB}	Volumetric TPB density (m^{-2})
μ	Gas viscosity (Pa s)
ν	Stoichiometric coefficient
ξ	Surface emissivity
ρ	Density (kg m^{-3})
σ	Electronic, ionic conductivity (S m^{-1})
σ_B	Stefan–Boltzmann constant (W m^{-2} K^{-4})
σ_k	Coordination number of k species
$\sigma_{\alpha\beta}$	Average collision diameter (Å)
τ_g	Tortuosity
$\vec{\tau}$	Stress tensor (Pa)
ϕ	Electronic, ionic potential (V)
ϕ_v	Viscous dissipation (kg m^{-1} s^{-3})
χ	Volumetric charge density (C m^{-3})
ψ	Volumetric charge source (C s^{-1} m^{-3})
$\Omega_{\alpha\beta}$	Collision integral

List of Subscripts and Superscripts

act	Activation
adv	Advection
an	Anode
cat	Cathode
chem	Chemical
con	Contact
conc	Concentration
diff	Diffusion
eff	Effective
eq	Equilibrium
irr	Irreversible
mol	Molecular
oc	Open-circuit
ohm	Ohmic
rad	Radiative
react	Reaction
res	Resistance
rev	Reversible

List of Acronyms

BV	Butler–Volmer
DGM	Dusty gas model
SMM	Stefan–Maxwell model
SOFC	Solid oxide fuel cell
SRU	Stack repeating unit
TPB	Three phase boundary

The scope of this chapter is to provide an introduction to solid oxide fuel cell (SOFC) modeling. A SOFC is a complex system consisting of three main components (electrolyte and porous electrodes, i.e., anode and cathode), each one composed of peculiar materials in which interconnected physical phenomena occur simultaneously involving gas and solid phases.

In SOFC applications, the individual cells are stacked together to increase the generated power, and if we consider the single unit of a stack of cells, which is called SRU (i.e., stack repeating unit), other components as interconnects, seals, and gas channels must be taken into account. Finally, if we look at the entire stack of cells, gas manifolds, insulation, and current collection plates have to be considered. Therefore, the modeling SOFC cells, SRUs, and stacks are the challenging tasks due to the wide variety of the components involved.

SOFC modeling can be carried out following different approaches, techniques, and levels of details depending on the objective of the model (e.g., cell performance simulation, study of the degradation of materials, and optimization of fluid distribution) and on the particular component or group of components on which the model is focused.

From a general point of view, SOFC systems (whether they are single cells, SRUs or stacks) can be considered as nonlinear dynamic systems with multiple inputs and outputs in which mass, momentum, energy, and charge transfer take place together with chemical and catalytic reactions. The goal of modeling is to develop mathematical tools capable of simulating the response of the system, with the purpose to provide models that can be applied to the design, analysis, control, or diagnostic of SOFC systems.

SOFC models can be generally classified into two main categories: experimentally based and physically based models (Wang et al. 2011a).

Experimentally based models of SOFC systems are developed using statistical data-driven approaches without applying equations derived from the knowledge of the involved physics. Regression-based and artificial neutral network techniques are applied to experimental databases in order to identify the relationship between inputs and outputs of the system that are implemented into predictive models which are mostly applied in the design of SOFC control strategies.

In the SOFC literature, most of the models are physically based. These models range from microscale (atomic or molecular level) to macroscale due to the fact that physical processes of SOFC systems have characteristic length and time scales from

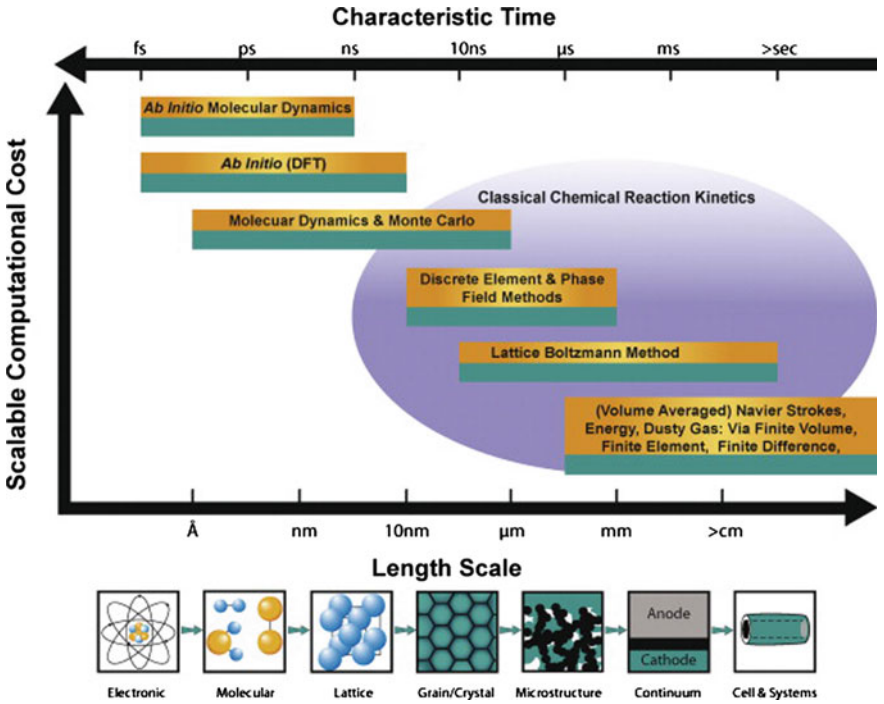

Fig. 1 Multidimensional SOFC modeling. [Reprinted with permission from Grew and Chiu (2012)]

angstrom and femtoseconds to centimeters and seconds. Consequently, the modeling techniques adopted strictly depend on the length and time scale of the described phenomena (Fig. 1).

At the scale of the electronic structure of matter, ab initio methods are used for the study of atomic interactions, followed by molecular dynamics and Monte Carlo techniques at the level of molecular structures, while discrete elements and phase field methods are adopted at the characteristic length of grain and crystals. Lattice Boltzmann Methods can be applied for the study of the fluid transport within microstructures, and finally the modeling methods that follow the continuum approach and use volume-averaged equations can be applied from the length scale of micrometers onwards to describe the physics of SOFC systems from the macroscopic point of view (Grew and Chiu 2012).

The modeling approaches presented in this chapter are physically based and focus on the macroscopic description of the phenomena.

In general, macroscopic models describe SOFC systems by using conservation laws and governing equations of the involved physics and range from 0-D to 3-D depending on the model objectives. Multidimensional models take into account the spatial distribution of the physical variables (temperature, species concentration, etc.) and are typically aimed at simulate cell/stack for design or optimization

purposes. The prediction of the steady state and transient response at cell, stack, and system level for diagnostic and control is frequently addressed by 0-D and 1-D models, due to their low computational cost.

When a macroscopic approach is adopted, many physical phenomena that are implicitly derived in the atomistic and molecular modeling are described by using empirical parameters. In particular, the representation of microscopic structures, chemical, and electrochemical kinetics is assigned to macroscopic parameters (e.g., porosity, tortuosity, and exchange current density) that can be estimated directly or indirectly (i.e., by fitting) from experimental measurements. Thus, in order to develop a physically based model, a representative set of experimental data is necessary.

Finally, physically based macroscopic models of SOFCs can follow two main goals: they can be oriented to the simulation of the performance or they can study the degradation processes occurring in the materials. In the first case, the models calculate system responses mainly in terms of voltage, current, temperature, chemical species, and pressure distributions; in the second, simulations focus on the calculation of thermal stresses, strain, and stress fields.

In the following sections, the discussion will be focused on the mathematical modeling of the physical phenomena that determine the SOFC performance. Transport and conservation of mass, momentum, charge, and energy are described and the basics of electrochemical and chemical reactions modeling are given.

1 Modeling the Mass Transfer in SOFCs

In SOFC systems, mass transfer takes place both in the gas phase (i.e., stack manifolds, gas channels, and porous electrodes) and in the solid phase (i.e., transport of ions in the electrolyte). The mass transfer of gases is studied in this section, while the transport of ions in the electrolyte is addressed in Sect. 4.

Mass transfer in the gas phase occurs by advection and diffusion. In general, mass transport and conservation can be expressed by using the continuity equation in the advection–diffusion form:

$$\frac{\partial \rho}{\partial t} + \nabla \cdot \left(\vec{j}_{\text{adv}} + \vec{j}_{\text{diff}}\right) = S \tag{1}$$

where ρ is the fluid density, t is the time, $\vec{j}_{\text{adv}}$ is the advective flux of mass due to the motion of the fluid, $\vec{j}_{\text{diff}}$ is the total diffusive flux of mass related to local gradients of temperature and partial pressures, and S accounts for the volumetric mass sources or sinks.

At the high operating temperatures of SOFC systems, fluids can be considered as ideal gases with a good approximation, thus the ideal gas law can be applied for the calculation of the fluid density:

$$\rho = \frac{pM_n}{RT} \tag{2}$$

where p is the total pressure of the gas mixture, M_n is the molecular weight of the mixture, T is the temperature, and R is the ideal gas constant.

The composition of gas mixtures in SOFC systems is not spatially homogeneous due to chemical and electrochemical reactions; moreover, a gas that moves in the electrodes can occupy only the void fraction of the porous domains. Hence, the mass transport Eq. (1) has to be re-elaborated in order to formulate a species balance that takes into account the porosity of materials and the mass fractions of chemical species in the gas mixture. For each component, the mass balance can be written as:

$$\frac{\partial(\varepsilon\rho x_\alpha)}{\partial t} + \nabla \cdot (\vec{j}_{\text{adv},\alpha} + \vec{j}_{\text{diff},\alpha}) = S_\alpha \tag{3}$$

where ε is the porosity and x_α is the mass fraction of the α component. Equation (3) is also valid in non-porous domains, where the porosity assumes the value of 1. For non-porous domains, the advective term of Eq. (3) can be expressed as:

$$\vec{j}_{\text{adv},\alpha} = \rho x_\alpha \mathbf{u} \tag{4}$$

where $\mathbf{u}$ is the fluid velocity field. In porous media, the advection term can be written as:

$$\vec{j}_{\text{adv},\alpha} = \rho x_\alpha \bar{\mathbf{u}} \tag{5}$$

where $\bar{\mathbf{u}}$ is the superficial velocity of the fluid in the porous domain (also called velocity of permeation, filtration or Darcy velocity). The superficial velocity is given by the Dupuit–Forchheimer relationship: $\bar{\mathbf{u}} = \varepsilon\mathbf{U}$, being $\mathbf{U}$ the mean velocity of the fluid through the pore space of the electrode, obtained by averaging the fluid velocity over a macroscopic volume of the electrode (Nield and Bejan 2006).

The source term of Eq. (3) accounts for the net volumetric production of the α species due to the electrochemical and chemical reactions. In general, S_α is given by:

$$S_\alpha = M_\alpha \sum_i \gamma_{si} \nu_{\alpha i} r_i \tag{6}$$

where r_i is the molar rate of the i-reaction, $\nu_{\alpha i}$ is the net stoichiometric coefficient of α species in the i-reaction, and γ_{si} is a scaling factor that assumes either a unitary value if the i-reaction rate is given per unit volume or it has the unit of inverse length (i.e., surface area per unit volume) if the i-reaction has a rate expressed per unit surface.

The molar rates of electrochemical reactions are given by the Faraday's law:

$$r_i = \frac{|i_v|}{nF} \tag{7}$$

where F is Faraday's constant, n is the number of electrons released during the reaction of one fuel molecule, and i_v is the volumetric current density. The calculation of the current density requires an electrochemical model that describes the charge-transfer chemistry in the SOFC electrodes, this topic will be treated in Sect. 4.

The molar rates of chemical reactions can be calculated from the study of global or detailed reaction mechanisms, as described in Sect. 5.

The electrochemical reactions involve limited regions of electrodes where charge-transfer reactions occur on the electrochemically reactive sites characterized by the coexistence of electron and ion conductor phases in the presence of gas-phase reactants. These regions are called triple- or three-phase boundaries (TPBs) and spread from the electrode/electrolyte interface of SOFCs into the electrode volume. In anode-supported cell models, the three-phase boundary is frequently assumed as a layer of negligible thickness at the anode/electrolyte interface (Costamagna et al. 2004; Ni 2009; Laurencin et al. 2011; Ferrero et al. 2015) and the mass sources due to the electrochemical reactions are imposed as boundary conditions at the border between electrode and electrolyte, instead of being included in the source term S_α.

Chemical reactions take place within the gas phase (i.e., homogeneous reactions) or on the surface of the solid medium of the electrode that acts as a catalyst for the reactions (i.e., heterogeneous reactions). In both cases, the volume in which chemical reactions occur covers the entire domain of SOFCs electrodes, and the reaction rates must be included in the volumetric source term of Eq. (3).

As stated before, the total diffusive flux of mass is due to the presence of temperature and partial pressures gradients. The thermal diffusion can be easily highlighted:

$$\vec{j}_{\mathrm{diff},\alpha} = \vec{j}_{\mathrm{d},\alpha} - D_{\alpha,\mathrm{T}} \frac{\nabla T}{T} \tag{8}$$

where $D_{\alpha,\mathrm{T}}$ is the thermal diffusion coefficient. The thermal diffusion of mass is also referred to as the Soret effect, which occurs in mixtures with high temperature gradients and large variations in molecular weight of the species. This type of diffusion is always neglected in SOFC models. The diffusive flux $\vec{j}_{\mathrm{d},\alpha}$ related to partial pressure gradients of the species will be described in detail in the following sections, where different diffusion models are introduced.

The solution of the mass balances requires to combine Eqs. (3) and (2) with a momentum balance (see Sect. 2) for the determination of the fluid velocity field, with a gas diffusion model for the calculation of the diffusive fluxes of the species, with an energy balance (see Sect. 3) for the determination of the temperature

distribution, and also with electrochemical and chemical models (see Sects. 4 and 5), which are required for the calculation of the species source term [see Eq. (6)].

As will be shown later, some gas diffusion models for the porous media [i.e., Fick's model in the advection–diffusion form (22) and dusty gas model (29)] already include the momentum balance. In these models, the mass flux determined by Eq. (5)—usually expressed as a function of the total pressure gradient by the application of Darcy's law (38) for the conservation of momentum—is included in the calculation of the total diffusive flux and referred to as a viscous flux.

The modeling of the gas diffusion depends on the medium where the diffusion occurs (i.e., porous or non-porous) and on the characteristics of the gas mixture (i.e., binary or multicomponent).

Before introducing the mathematical description of the diffusive flux $\vec{j}_{\mathrm{d},\alpha}$, a brief presentation of the diffusive models is given.

In the SOFC literature, three theoretical models are usually applied to describe the diffusive mass transport: Fick model, Stefan–Maxwell model, and dusty gas model.

Diffusion models based on Fick's law assume that the flux of a chemical species in a gas mixture is proportional to its concentration gradient. These models are often presented in the advective-diffusive form, in which molecular diffusion due to concentration gradients and viscous flow due to pressure gradients are linearly combined (Webb and Pruess 2003). Fick's law is rigorously valid only for binary mixtures or in the case of diffusion of dilute species in a multicomponent mixture (Krishna and Wesselingh 1997; He et al. 2014a, b), and its application to the diffusion in porous media is consistent in a very narrow range of conditions (Bertei and Nicolella 2015). Nevertheless, Fick-based models are widely employed not only in modeling the diffusion in binary mixtures, but also in the modeling of concentrated species diffusion in multicomponent mixtures in both porous and non-porous media, due to their simplicity (Ferguson et al. 1996; Ho et al. 2008, 2009; Goldin et al. 2009; Elizalde-Blancas et al. 2013).

The Stefan–Maxwell model is frequently used in the literature to overcome the limitations of Fick's law (Krishna and Wesselingh 1997; Suwanwarangkul et al. 2003). This model is derived from the kinetic theory and correctly describes the multicomponent diffusion in non-porous domains, but it does not include the interaction between pore walls and gas molecules (Webb and Pruess 2003; Suwanwarangkul et al. 2003). In some diffusion models, the Stefan–Maxwell equations have been modified to include the gas-pore interactions, as in the binary friction model of Kerkhof (1996) or in the work of Hussain et al. (2005).

The dusty gas model (Mason and Malinauskas 1983), which takes into account both the interactions between the different components of a gas mixture and the gas–wall collisions, has proven to be the most suitable and rigorous model for the description of multicomponent diffusion in porous media (Suwanwarangkul et al. 2003; Hernández-Pacheco et al. 2004). Even if it has the higher predictive capability, the dusty gas model is not widely applied as the Fick's one due to its complexity. In particular, Fick and Stefan–Maxwell models can be solved

analytically by deriving explicit expressions for the diffusion fluxes, while the dusty gas model requires a numerical solution (Suwanwarangkul et al. 2003). For this reason, the dusty gas model is frequently presented in simplified forms in the SOFC literature, usually by assuming uniform pressure in the electrodes (Jiang and Virkar 2003; Hernández-Pacheco et al. 2004; Janardhanan and Deutschmann 2006; Matsuzaki et al. 2011; Geisler et al. 2014; Ferrero et al. 2015), and in the work of Kong et al. (2012) it has been reformulated in the form of a Fickian model in order to facilitate its implementation.

Modeling diffusion in non-porous domains: Fick and Stefan–Maxwell models

In the non-porous domains (i.e., gas channels and manifolds), $\vec{j}_{d,\alpha}$ is the mass flux originated by the molecular diffusion of the species α in the gas mixture that can be binary (i.e., typically air in the cathode channels) or multicomponent. The molecular diffusion (also called continuum or ordinary diffusion) is due to the relative motion of the different species of the gas mixture driven by partial pressure gradients. For the diffusion modeling in non-porous media, Fick and Stefan–Maxwell models are usually applied in the literature.

The simplest diffusion model is the Fick's one. The model is given by (Bird et al. 2006):

$$\vec{j}_{d,\alpha} = -\rho D_{\alpha m} \nabla x_\alpha \tag{9}$$

where $D_{\alpha m}$ is the diffusivity of the species α in the gas mixture. For a binary mixture, $D_{\alpha m}$ coincides with the ordinary diffusion coefficient of the gas phase, $D_{\alpha\beta}$, which is independent of the gas mixture composition and can be calculated using the theoretical correlation of Chapman–Enskog (Poling et al. 2001):

$$D_{\alpha\beta} = \frac{0.00266}{\sqrt{2}} \left(\frac{1}{M_\alpha} + \frac{1}{M_\beta} \right)^{1/2} \frac{T^{3/2}}{p \sigma_{\alpha\beta}^2 \Omega_{\alpha\beta}} \tag{10}$$

where M_α and M_β are molecular weights, $\sigma_{\alpha\beta}$ is the average collision diameter, $\Omega_{\alpha\beta}$ denotes the collision integral, and p is the total pressure of the mixture (bar). In the literature, the empirical correlations of Fuller et al. (1966) are frequently used for the calculation of the binary diffusion coefficients:

$$D_{\alpha\beta} = \frac{0.00143 \cdot T^{1.75}}{p \left[\frac{2}{(1/M_\alpha + 1/M_\beta)} \right]^{1/2} \left[(\Sigma V_{aA})^{1/3} + (\Sigma V_{aB})^{1/3} \right]^2} \tag{11}$$

where ΣV_{ai} are the sums of the atomic diffusion volumes, p is the total pressure of the mixture (bar), and $D_{\alpha\beta}$ is expressed in ($cm^2\ s^{-1}$).

Many researchers have applied Fick's law to multicomponent diffusion modeling; in this case, the ordinary diffusivity of the species α in the gas mixture is usually given by the Wilke's formula (Yakabe et al. 2000; Wilke 1950a, b):

$$D_{\alpha m} = \frac{1 - y_\alpha}{\sum_{\beta \neq \alpha} \frac{y_\beta}{D_{\alpha\beta}}} \tag{12}$$

Equation (12) is strictly valid for the diffusion of gases in a stagnant multicomponent mixture. When this assumption is not satisfied, as in the case of diffusion in SOFC channels, manifolds, and electrodes, the solution of the system of Eq. (9) leads to an intrinsic flux inconsistency, i.e., the sum of the diffusive fluxes is not zero (Désilets et al. 1997). In order to overcome this drawback of the model, it is necessary to replace one of the Eq. (9) with the consistency condition:

$$\sum_{\forall \alpha} \vec{j}_{\mathrm{d},\alpha} = 0 \tag{13}$$

In this way, one of the diffusion mass fluxes is "artificially" calculated so that their sum gives zero. A consistent method that combines Fick's law and flux consistency has been proposed by Ramshaw (1990):

$$\vec{j}_{\mathrm{d},\alpha} = -\rho D_{\alpha m} \nabla x_\alpha + \rho x_\alpha \sum_{\forall \beta} (D_{\beta m} \nabla x_\beta) \tag{14}$$

The Stefan–Maxwell model describes the multicomponent mass transport following a rigorous theoretical approach that allows to correctly describe the counterdiffusion effects of ternary mixtures of gases. Stefan–Maxwell equations are formulated as force balances on the chemical species of a gas mixture. The equations are written as a balance between the driving force of the motion of a species (i.e., the partial pressure gradient) and the friction between that species and each of the other species of the mixture (Krishna and Wesselingh 1997). The equations are given by:

$$\sum_{\beta \neq \alpha} \frac{y_\beta \vec{J}_{\mathrm{d},\alpha} - y_\alpha \vec{J}_{\mathrm{d},\beta}}{D_{\alpha\beta}} = -\frac{p}{RT} \nabla y_\alpha \tag{15}$$

where $\vec{J}_{\mathrm{d},\alpha}$ is the molar diffusive flux relative to concentration gradients, and the Stefan–Maxwell diffusion coefficient $D_{\alpha\beta}$ is equal to the binary diffusion coefficient used for Fick's law (11). Equation (15) can be rearranged to show the mass diffusive fluxes:

$$\sum_{\beta \neq \alpha} \frac{M_n}{M_\beta} \left(\frac{x_\beta \vec{j}_{\mathrm{d},\alpha} - x_\alpha \vec{j}_{\mathrm{d},\beta}}{D_{\alpha\beta}} \right) = -\rho \nabla x_\alpha \tag{16}$$

It is worth noting that Stefan–Maxwell expressed with Eqs. (15)–(16) does not take into account the effect of total pressure gradients, as well as the Fick's model (9).

Some authors have proposed different diffusion models based on Stefan–Maxwell equations that also include the viscous effects due to the presence of a total pressure gradient.

In the works of Andersson et al. (2010), Stefan–Maxwell equations are formulated with a different approach (Curtiss and Bird 1999) that includes the total pressure gradient in the forces balance on the gas species:

$$\vec{j}_{\mathrm{d},\alpha} = -\left(\rho x_\alpha \sum_i D_{\alpha i} \boldsymbol{d}_i\right) \tag{17}$$

where $\boldsymbol{d}_i$ is the diffusional driving force:

$$\boldsymbol{d}_i = \nabla y_i + \frac{1}{p}\left[(y_i - x_i)\nabla p\right] \tag{18}$$

In the work of Novaresio et al. (2012), Stefan–Maxwell equations are derived by using a thermodynamic approach in which partial pressure gradients are expressed as the sum of the pressure gradients due to diffusive and viscous effects. The equation obtained is given by:

$$\frac{1}{RT}\nabla p_\alpha = \sum_{\beta \neq \alpha} \frac{y_\alpha \vec{J}_{\mathrm{d},\beta} - y_\beta \vec{J}_{\mathrm{d},\alpha}}{D_{\alpha\beta}} + \frac{1}{RT} x_\alpha \nabla p \tag{19}$$

For a multicomponent mixture composed of n gases, the Stefan–Maxwell model expressed by (15), (17), or (19) is a system of n equations in the n flux unknowns. However, only $n - 1$ of the equations are linearly independent (Ramshaw 1990). Thus, the flux consistency (13) has to be imposed to close the system of equations.

Finally, it is worth noting that both the Fick and Stefan–Maxwell models presented in this section do not comprise a momentum balance; thus, in the formulation of the complete mass transport model for the fluid, the momentum conservation equations have to be added. A complete comparison of the performance between Fick's and Stefan–Maxwell models is given in the works of Krishna and Wesselingh (1997) and Suwanwarangkul et al. (2003).

Modeling diffusion in porous domains: Fick and dusty gas models The prediction of partial pressure profiles within porous electrodes is of paramount importance to allow the correct estimation of current density, electrode potential, and local reaction rates in a cell model. In order to correctly model the gas transport in SOFC electrodes, it is necessary to describe the motion of gas mixtures in porous media by taking into account the interactions of the gas species among themselves and with the walls of the pores.

The mass transport of gases in porous media is generally described by three mechanisms: viscous flow, molecular diffusion, and Knudsen diffusion. The viscous flow is related to total pressure gradients, the molecular diffusion to partial

pressure gradients, and the Knudsen diffusion is produced by both type of gradients combined with molecule-pore wall collisions. The transport of adsorbed gas molecules on the solid surfaces of pores is another transport mechanism that takes place in porous structures; however, its contribution to the diffusivity is usually neglected (Froment et al. 1990; Kast and Hohenthanner 2000).

In order to identify the type of transport mechanism that is dominant in the porous electrode, the Knudsen number is usually adopted (He et al. 2014a, b):

$$Kn = \frac{\lambda}{L_{\mathrm{p}}} \tag{20}$$

where λ is mean free path of gas molecules and L_{p} is the characteristic size of the pore, typically its diameter if pores are assumed as spherical. The mean free path of a gas molecule can be directly calculated from the kinetic theory:

$$\lambda = \frac{k_{\mathrm{B}} T}{\sqrt{2} p \pi d_{\mathrm{mol}}^2} \tag{21}$$

where d_{mol} is the molecule diameter and k_{B} is the Boltzmann constant.

Depending on the value assumed by the Knudsen number, three different flow regimes can be identified: a continuum regime for Kn smaller than 0.01, a transition regime for Kn in the range of 0.01–10, and a Knudsen regime when Kn is larger than 10.

Molecular diffusion and viscous flow are the dominant mechanisms in the continuum regime; in this case, the momentum transfer occurs by collisions between molecules, which are more frequent than the surface collisions between molecules and pore walls. In the continuum regime, concentration gradients lead to mass transfer due to molecular diffusion and a total pressure gradient produces a viscous flow.

In the Knudsen regime, the molecule-pore collisions are more frequent than the intermolecular collisions, and the momentum transfer is determined by the interactions between molecules and pore walls. In this regime, a gradient of pressure or concentration leads to a mass transfer due to Knudsen flow, as there is no distinction between flow and diffusion in a non-continuum regime (Kast and Hohenthanner 2000).

In an SOFC electrode, the gas flow takes place in a transitional regime, as the mean pore diameter usually ranges between 0.4 and 2.6 μm (Funahashi et al. 2007; Greene et al. 2006; Hao et al. 2008; Jung et al. 2006; Lanzini et al. 2009; Moon et al. 2008; Park et al. 2009; Yakabe et al. 2000; Zhu and Kee 2003) and the mean free path for typical SOFC gases and operating conditions is about 0.2–0.5 μm (Hirschfelder et al. 1954); thus, in the presence of concentration and pressure gradients, all the three mechanisms must be taken into account.

For the diffusion modeling in porous media, Fick and dusty gas model are usually applied in the literature.

The Fick model given by Eq. (9) is also applied in the porous media. In order to consider the viscous diffusion, the model is frequently presented in the advective-diffusive form (Webb and Pruess 2003):

$$\vec{j}_{d+a,\alpha} = -\rho\left(D^{\text{eff}}_{\alpha mK}\nabla x_\alpha + \frac{B_p x_\alpha}{\mu_g}\nabla p\right) \tag{22}$$

where B_p is the permeability of the porous medium, μ_g is the gas viscosity, and $D^{\text{eff}}_{\alpha mK}$ is the effective diffusive coefficient which takes into account both the molecular and Knudsen diffusivity. The permeability can be expressed by thy Kozeny–Carman relationship (Bear 1972), which is based on the assumption that the porous electrode is formed by closely packed spherical particles:

$$B_p = \frac{\varepsilon^3 d_p^2}{72\tau_g(1-\varepsilon)^2} \tag{23}$$

where τ_g is the tortuosity parameter and d_p is the diameter of the particles (μm). Firstly introduced by Carman (1956), the tortuosity takes into account the complexity of the diffusion path of a fluid inside the porous media and can be defined as the ratio between the lengths of real diffusion path and straight path. There is a strong disagreement in the literature about the value of the tortuosity in fuel cell electrodes; the survey of Brus et al. (2014) shows values between 1 and 10 and indicates that the most precise estimations of tortuosity can be derived from the image analysis of real electrodes obtained by FIB–SEM methods (Lanzini et al. 2009; Wilson et al. 2011; Joos et al. 2011; Lee et al. 2013; Iwai et al. 2010; Kishimoto et al. 2011) (Fig. 2).

Using these techniques, the typical tortuosity of SOFC anodes is in the range of 1.5–4 (Brus et al. 2014).

The Knudsen diffusivity of the gas species α in a porous media is given by Lehnert et al. (2000):

$$D_{K,\alpha} = \frac{d_\varepsilon}{3}\sqrt{\frac{8RT}{\pi M_\alpha}} \tag{24}$$

where d_ε is the mean pore size of the porous media (μm).

The molecular and Knudsen diffusion coefficients can be combined in a global diffusion coefficient (Welty et al. 2001):

$$\frac{1}{D_{\alpha mK}} = \frac{1}{D_{K,\alpha}} + \frac{1-\Upsilon y_\alpha}{D_{\alpha m}} \tag{25}$$

The coefficient Y is usually assumed to be zero in the SOFC literature, leading to the Bosanquet formula (Suwanwarangkul et al. 2003; Pollard and Present 1948; Veldsink et al. 1995):

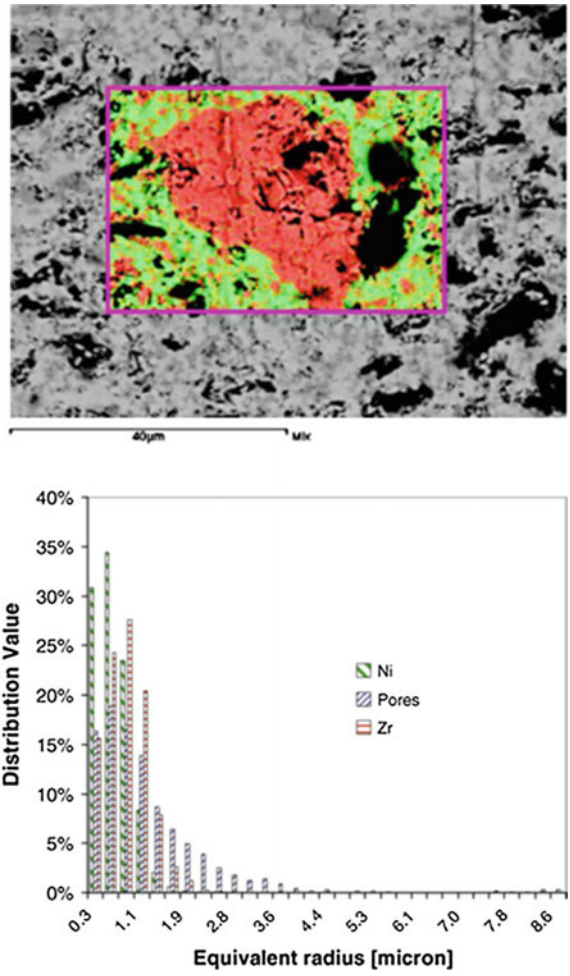

Fig. 2 Microstructural characterization of SOFC: in the *upper panel*, the EDS element mapping of Ni/YSZ anode regions (*red* Ni, *green* Zr, *black* pore); in the *lower panel*, the average phase distribution of the anode. [Reprinted with permission from Lanzini et al. (2009)]

$$D_{\alpha mK} = \left(\frac{1}{D_{K,\alpha}} + \frac{1}{D_{\alpha m}} \right)^{-1} \tag{26}$$

The Bosanquet relation is based on diffusion in aligned cylindrical pores, and it does not take into account the real geometry of the electrode structure in which gases diffuse through convoluted paths. The effective diffusivity has been studied by Bruggeman (1935) who analyzed the properties of various heterogeneous substances. If the porous electrode is assumed as composed of a solid phase made of spheres and the bed phase surrounding the spheres is treated as the void fraction of the electrode, the Bruggeman's equation for the diffusivity can be used:

$$D_{\alpha mK}^{\text{eff}} = \varepsilon^{1.5} D_{\alpha mK} \tag{27}$$

In the SOFC literature, the effective diffusivity is usually presented (Chan et al. 2001; Hajimolana et al. 2011) in a different form, which takes into account the tortuosity of the porous structure:

$$D_{\alpha mK}^{\text{eff}} = \frac{\varepsilon}{\tau_{\text{g}}} D_{\alpha mK} \tag{28}$$

In the work of Webb and Preuss (2003), the Knudsen diffusion is included in the advective-diffusive form of the Fick model through the use of the Klinkenberg factor to obtain an effective permeability, while in the first term of Eq. (22), the effective diffusivity used does not include the Knudsen effect.

As stated before, numerous studies have shown the limitations and drawbacks of the use of Fick's law to predict the diffusion fluxes for multicomponent mixtures in porous media. In particular, the work of Bertei and Nicolella (2015) has pointed out how the use of Bosanquet formulation, which is strictly valid for self-diffusion or equimolar counter transfer (Welty et al. 2001), can lead to inconsistent results in the diffusive flow calculations.

The dusty gas model is derived from the kinetic theory and treats the porous medium as one component of the gas mixture. The medium is assumed as a gaseous phase of giant molecules (the "dust") uniformly distributed in the porous domain, motionless and with infinite molar mass (Krishna and Wesselingh 1997). By applying the Stefan–Maxwell equations to this mixture, the transport of gases is described by an implicit expression that includes the effect of concentration and total pressure gradients (Mason and Malinauskas 1983):

$$-\frac{1}{RT}\nabla p_\alpha = \sum_{\beta \neq \alpha} \frac{y_\beta \vec{J}_\alpha - y_\alpha \vec{J}_\beta}{D_{\alpha\beta}^{\text{eff}}} + \frac{\vec{J}_\alpha}{D_{K\alpha}^{\text{eff}}} + \frac{1}{D_{K\alpha}^{\text{eff}}} \frac{p_\alpha}{RT} \frac{B_{\text{p}}}{\mu_{\text{g}}} \nabla p \tag{29}$$

where $D_{\alpha\beta}^{\text{eff}}$ and $D_{K\alpha}^{\text{eff}}$ are the effective multicomponent and Knudsen diffusivities, directly calculated from $D_{\alpha\beta}$ and $D_{K,\alpha}$ by using (27) or (28). The dusty gas model includes the momentum balance in the form of Darcy's Law, as can be seen from the last term of Eq. (29), which is the viscous flow, and intrinsically ensures the flux consistency. A large number of studies have shown the validity of the dusty gas model (Krishna and Wesselingh 1997; Veldsink et al. 1995; Tseronis et al. 2008; Wang et al. 2012) for multicomponent flows in porous media.

In the work of García-Camprubí et al. (2010), the total flux of a species in a multicomponent mixture obtained from the application of the dusty gas model has been expressed as the contribution of three terms:

$$\vec{J}_\alpha = -\Gamma_\alpha \nabla p_\alpha + \vec{v}_\alpha^{\,p} p_\alpha + \vec{v}_\alpha^{\,N} p_\alpha \tag{30}$$

where

$$\Gamma_\alpha = \frac{1}{RT\left[\sum_{\beta\neq\alpha}\left(\frac{p_\beta}{D^{\text{eff}}_{\alpha\beta}}\right) + \frac{1}{D^{\text{eff}}_{K\alpha}}\right]} \tag{31}$$

$$\vec{v}^{p}_{\alpha} = \frac{\Gamma_\alpha}{D^{\text{eff}}_{K\alpha}}\left[-\frac{B_{\text{p}}}{\mu_{\text{g}}}\nabla p\right] \tag{32}$$

$$\vec{v}^{N}_{\alpha} = \Gamma_\alpha RT\sum_{\beta\neq\alpha}\left[\frac{\vec{J}_\beta}{pD^{\text{eff}}_{\alpha\beta}}\right] \tag{33}$$

The first term represents the total diffusion of the species related to concentration gradients (i.e., a purely diffusive term), the second is the viscous flux due to pressure gradients, and the third is the flow of the species α induced by the motion of the other species. The last term, peculiar of the dusty gas model and totally neglected by Fick-based models, has a growing importance with the increasing of the current density. For this reason, the application of dusty gas model is recommended (Suwanwarangkul et al. 2003; Cayan et al. 2009) for predicting concentration overpotentials in SOFC models in the polarization regions where limiting currents occur due to the presence of high current densities and low concentration of electrochemical reactants.

The implicit formulation of fluxes and the presence of a term dependent on the pressure gradient make it difficult to solve the equations of dusty gas model. Therefore, many authors assume the viscous flow to be negligible and use the model in combination with the momentum equation given by Darcy's Law. However, the dusty gas model applied with the uniform pressure simplification no longer guarantees the flux consistency, and Eq. (13) must be applied to calculate the flux of one species. In particular, Bertei and Nicolella (2015) have shown that the uniform pressure assumption is equivalent to assume the Graham's law of effusion, which is rigorously valid only in a confined system in the absence of reactions and pressure gradients, conditions that are not satisfied in an SOFC electrode.

2 Momentum Conservation

The momentum conservation equations derive directly from the application of the second Newton's law of motion. Mathematically, the momentum conservation in the non-porous domains (i.e., gas channel and manifolds) is described by the Navier–Stokes equations for compressible fluids:

$$\frac{\partial(\rho \boldsymbol{u})}{\partial t} + \nabla \cdot (\rho \boldsymbol{u}\boldsymbol{u}) = -\nabla p + \nabla \cdot \vec{\tau} + \boldsymbol{F} \tag{34}$$

where $\boldsymbol{F}$ are the body forces (e.g., gravity and electromagnetic forces.) and $\vec{\tau}$ is the stress tensor. Equation (34) represents a force balance on the fluid particles; it states that the total force applied to the particles is the sum of three contributions: pressure, stress, and external forces. The external forces in SOFC channels are usually neglected. For a Newtonian compressible fluid, the stress tensor is given by:

$$\vec{\tau} = \left[\mu_{\mathrm{g}}\left(\nabla \boldsymbol{u} + (\nabla \boldsymbol{u})^T\right) - \frac{2}{3}\mu_{\mathrm{g}}(\nabla \cdot \boldsymbol{u})\right] \tag{35}$$

where μ_{g} is the dynamic viscosity of the fluid. This property can be estimated through the combination of the viscosities of single components by using the Wilke's formula (Wilke 1950a, b):

$$\mu = \sum_{\forall i}\left[\frac{y_i \mu_i}{\sum_{\forall j}\left(y_j \theta_{ij}\right)}\right] \tag{36}$$

where θ_{ij} is given by the equation:

$$\theta_{ij} = \frac{\left[1 + \left(\frac{\mu_i}{\mu_j}\right)^{1/2}\left(\frac{M_j}{M_i}\right)^{1/2}\right]^2}{(4/\sqrt{2})\left[1 + \left(\frac{M_i}{M_j}\right)\right]^{1/2}} \tag{37}$$

The fluid flow through porous media is characterized by convoluted paths, and it is not possible to apply the classical laws of mechanics separately to fluid and solid phases, due to the complex configuration of the contact boundaries between the phases. A continuum approximation has to be applied in order to formulate the momentum balance, and the macroscopic equations are derived by using averaging methods.

Several approaches have been proposed to formulate the momentum balance through a porous media; in the simplest form, the momentum conservation is expressed by Darcy's law, which assumes a linear proportionality between the flow velocity and the applied pressure difference:

$$\bar{\boldsymbol{u}} = -\frac{B_{\mathrm{p}}}{\mu_{\mathrm{g}}}\nabla p \tag{38}$$

This equation describes the balance on the fluid between the force applied by the pressure gradient and the frictional resistance due to the presence of a porous medium. In the Darcy's equation, the inertia forces are neglected, and the validity of the model is limited to laminar flows in low-porosity media dominated by viscous

forces. Typically, the linear relation of Darcy's equation is valid for Reynolds number of the flow in the order of unity or smaller (Nield and Bejan 2006).

An extension of the Darcy model to high velocity flows in porous media, or to high porosity media, is given by the Forchheimer's equation:

$$\nabla p = -\frac{\mu_g}{B_p}\bar{\boldsymbol{u}} - C_f \rho \frac{|\bar{\boldsymbol{u}}|\bar{\boldsymbol{u}}}{\sqrt{B_p}} \tag{39}$$

where C_f is a dimensionless drag constant. The last term of Eq. (39) is referred to as Forchheimer term and takes into account the inertia effects in the fluid flow. The C_f coefficient varies with the characteristics of the porous medium; a thorough discussion on the several different approaches adopted in the literature for the evaluation of this coefficient can be found in Nield and Bejan (2006).

The main limitation of the Darcy and Forchheimer equations is the impossibility to impose the no-slip boundary condition (Amhalhel and Furmański 1997). Hence, when Eqs. (38) or (39) is imposed in the porous medium, it is difficult to define interfacial conditions with an adjacent domain in which there is a free-flow and Navier–Stokes equations are applied, as typically happens at the electrode/channel interface of SOFC cells (Andersson et al. 2010).

The Brinkmann–Darcy flow model can be adopted to overcome the limitations of Darcy–Forchheimer equations. The Brinkmann–Darcy equations are given by Brinkman (1949a, b):

$$\nabla p = -\frac{\mu_g}{B_p}\bar{\boldsymbol{u}} + \tilde{\mu}_g \nabla^2 \bar{\boldsymbol{u}} \tag{40}$$

where $\tilde{\mu}_g$ is an effective dynamic viscosity that Brinkman set equal to the gas viscosity. More recent studies have shown that the effective viscosity is a function of the characteristic of the porous medium, in particular of the porosity (Amhalhel and Furmański 1997; Nield and Bejan 2006). The Brinkman–Darcy flow model allows to account for all boundary conditions at a solid or fluid interface.

A generalized flow model that includes the Forchheimer term into the Brinkman–Darcy equation has been derived by Hsu and Cheng (1990) starting from the Navier–Stokes equations and utilizing volume-averaging techniques:

$$\frac{1}{\varepsilon}\left[\frac{\partial(\rho\bar{\boldsymbol{u}})}{\partial t} + \nabla\cdot\left(\frac{\rho}{\varepsilon}\bar{\boldsymbol{u}}\bar{\boldsymbol{u}}\right)\right] = -\nabla p + \nabla\cdot\left(\frac{\bar{\boldsymbol{\tau}}}{\varepsilon}\right) + \mu_g\nabla^2\bar{\boldsymbol{u}} - \frac{\mu_g}{B_p}\bar{\boldsymbol{u}} - C_f\rho\frac{|\bar{\boldsymbol{u}}|\bar{\boldsymbol{u}}}{\sqrt{B_p}} + \frac{\boldsymbol{F}}{\varepsilon} \tag{41}$$

Equation (41) is known as Darcy–Brinkman–Forchheimer (DBF) flow model. In the work of Lage (1993), a complete study on the influence of each term of the DBF equation depending on the flow regime is presented.

The Darcy–Brinkman–Forchheimer equation is the most complete formulation of momentum conservation in the porous medium. When the free-flow

approximation (i.e., infinite permeability and $\varepsilon = 1$) is applied in Eq. (41), the equation reduces to the Navier–Stokes form (34). Therefore, when modeling a fuel cell, it is possible to apply Eq. (41) in both free-flow and porous-medium domains. With this approach, the velocity field is continuous in the entire domain and coupling conditions between porous electrodes and free channels are not need. The Darcy–Brinkman flow model (with or without the Forchheimer term) is the standard model used by many CFD softwares (Fluent, COMSOL Multiphysics, OpenFOAM, etc.) to deal with fluid transport problems in porous media.

3 Energy Transport and Conservation

Modeling the heat transfer in SOFC systems allows the prediction of temperature distribution within cells and stacks, which is necessary for an accurate simulation of cell performance and for the prediction of thermo-mechanical degradation of cells and stack components.

Heat transport models must take into account the different heat transfer mechanisms, namely convective heat transfer between solid surfaces and gas mixtures, conductive heat transfer in gaseous and solid phases, and radiative heat transfer. Moreover, energy conservation equations must include the presence of heat sources (or sinks) due to chemical and electrochemical reactions, and the heat production due to the motion of electronic and ionic charges.

The conservation of energy can be implemented in a model by applying the first law of thermodynamics, which assumes different forms depending on the heat transfer phenomena that dominate the domain under investigation.

In the following part of the section, the equations describing heat transfer and conservation are introduced by type of domain from the non-porous fluid and solid domains to the porous domains of the electrodes.

Heat transfer in non-porous media: fluid domains The general form of the energy conservation equation for the heat transfer in a fluid domain is given by the enthalpy conservation equation, which can be expressed in terms of temperature, as follows:

$$\frac{\partial\left(\rho C_{\mathrm{p}} T\right)}{\partial t} + \nabla \cdot \left(\rho C_{\mathrm{p}} T \boldsymbol{u}\right) + \nabla \cdot \vec{q} = \frac{Dp}{Dt} + \phi_{\mathrm{v}} + \rho \boldsymbol{f}\boldsymbol{u} + Q \tag{42}$$

where $\vec{q}$ is the heat flux by conduction, ϕ_{v} is the viscous dissipation, $\boldsymbol{f}$ are the specific body forces acting on the fluid (e.g., gravity), and Q represents the volumetric heat sources. The energy dissipation due to viscous forces is important for highly viscous fluids at high velocity but is negligible for gas flows under the typical laminar regimes of SOFCs. Also the pressure work may be neglected, since the pressure differences of fuel cells are very small. Moreover, it can be assumed

with a good approximation that the body forces are irrelevant in the energy balance. Thus, Eq. (42) can be rewritten as follows:

$$\frac{\partial\left(\rho C_{\mathrm{p}} T\right)}{\partial t} + \nabla \cdot \left(\rho C_{\mathrm{p}} T \boldsymbol{u}\right) + \nabla \cdot \vec{q} = Q \tag{43}$$

The conductive heat transfer is given by the Fourier's law:

$$\vec{q} = -k_{\mathrm{g}} \nabla T \tag{44}$$

where k_{g} is the thermal conductivity of the gas mixture. This property can be calculated by the Wilke's formula [see Eq. (36)], as in the case of the viscosity.

The volumetric heat sources in fluid domains are chemical reactions and radiative heating. The latter heating mechanism is related to the absorption, scattering, and emission of radiation by the fluid that occurs in the presence of participating gases.

The heat source term is negligible when considering the cathodic fluids of SOFCs, because they are composed of non polar molecules (i.e., oxygen and nitrogen) that do not react with each other and that can be considered as transparent gases non-interacting with thermal radiation at the conditions of SOFC applications.

Chemical reactions between the typical fuel mixture components (i.e., H_2, H_2O, CO, CO_2, and CH_4) at SOFC operating conditions occur when the gas flow comes in contact with suitable catalysts, as typically happens within the porous structure of the anode. The studies of Gupta et al. (2006) and Walters et al. (2003) have shown that homogeneous reactions cannot be ignored in non-catalytic regions of SOFCs only with particular fuel mixtures, specifically air/methane and dry natural gas. However, if we consider the typical fuel mixtures in stack manifolds and cell channels, chemical reactions between components can be neglected. Moreover, the calculated gas transmittance for a typical SOFC fuel stream composition at atmospheric pressure yields a value approaching unity (Damm and Fedorov 2005); thus, the fuel gas medium can be treated as transparent. Hence, the Q term is negligible for both anodic and cathodic gas mixtures in the non-porous domains of a SOFC system.

Once the conservation equation has been imposed in the fluid domains of the model, proper boundary conditions have to be chosen.

The conditions imposed at the boundaries of fluid domains strictly depend on the geometry and assumptions of the model. Most the models impose a fixed temperature at the fluid inlets and a convective flux at the outlets. Typical boundary conditions at the walls of fluid domains are thermal insulation, convective heat transfer, continuity of the temperature field across the boundary, or periodic boundary conditions, depending on the model. Even if heat transfer by radiation is not included into the energy conservation equation, the radiative exchange between the surfaces of channel and manifolds should be considered when defining the boundary conditions at the walls of the fluid domains. The surface-to-surface radiation is usually modeled using view-factor methods (Sánchez et al. 2007;

Damm and Fedorov 2005), and the radiative flux for an infinitesimal element of a surface is given by (García-Camprubí 2011):

$$\vec{q}_{\mathrm{rad},i} = \xi_i \left[E_{\mathrm{b},i} - \sum_j \left(F_{i-j} E_{\mathrm{b},j} \right) - H_{0,i} + \sum_j \left[\left(\frac{1}{\xi_j} - 1 \right) F_{i-j} q_{\mathrm{rad},j} \right] \right] \vec{n} \tag{45}$$

where ξ is the emissivity of the surface, E_b is the emissive power of a black body, H_0 is the incident radiation, and F_{i-j} is the view factor between two infinitesimal elements i and j. The view factor of Eq. (45) represents the fraction of radiation emitted by the surface element i that is directly incident on the element j. In the case of domains with high aspect ratio, typical of planar-type SOFC channels, the walls can be treated as black surfaces with unitary emissivity (i.e., $\xi_i = 1$). The radiative heat flux calculated at the surface can be then imposed as a boundary flux:

$$-\nabla \cdot (k \nabla T) = \nabla \cdot \vec{q}_{\mathrm{rad}} \tag{46}$$

The modeling study of Yakabe et al. (2001) on a planar SOFC has shown that when the surface-to-surface heat exchange is taken into account, the temperature distribution in the cell is flatter and the maximum temperature is 30 °C lower with respect to profiles obtained without considering the radiant heat exchange.

Heat transfer in non-porous media: solid domains In the solid domains of SOFC systems (i.e., electrolyte, interconnects, and other impervious stack components), conduction is the dominant heat transfer mechanism, and radiation can play a role, while the convection is negligible since the material is not moving. In the absence of convective terms, the energy conservation equation is given by:

$$\frac{\partial \left(\rho C_\mathrm{p} T \right)}{\partial t} + \nabla \cdot \vec{q} = Q_\mathrm{v} \tag{47}$$

In order to determine whether or not to include radiation in the heat transfer model of solid domains, it is necessary to evaluate the magnitude of the heat transfer by radiation and compare it with that of the conductive heat flux. A simple evaluation method is suggested by Damm and Fedorov (2005), which is based on the comparison of the maximum possible heat flux exchanged by radiation between two black walls separated by a transparent medium with the conductive flux calculated by the Fourier's law. If the magnitude of the radiation is not negligible, the heat flux exchanged by radiation should be included in Eq. (47) into the source or heat flux terms.

The radiative heat flux can be calculated by solving the radiative transfer equation (RTE) (Modest 2013). The RTE is an integro-differential equation, whose analytic solution exists only for few simple cases, and its numerical solution has a high computational cost; thus, the radiative flux is usually evaluated using approximate solutions of the RTE.

If the material is optically thin, radiation can be included in the energy conservation equation as a volumetric source that is accounted for in the Q_v term. In

Eq. (47), the total volumetric heat source Q_v can be expressed as the sum of the Joule heating, which occurs in electrically conductive materials traversed by ionic or electronic current, and the radiative heating. Electrochemical and chemical reactions take place in the electrode domains and should not be accounted for in the source term. The resulting total source is given by:

$$Q_v = Q_{ohm} + Q_{rad} = \frac{\left|i_{e/i}\right|^2}{\sigma_{e/i}} - \nabla \cdot q_r. \tag{48}$$

where $\sigma_{e/i}$ is the ionic/electronic conductivity of the material, $\left|i_{e/i}\right|$ is the local current density (see Sect. 4), and q_r is the radiative heat flux, which derives from approximate solutions of the RTE, for example the Schuster–Schwartzchild two-flux approximation in the case of 1-D models (Murthy and Fedorov 2003). The traditional YSZ electrolyte of SOFCs can be considered as an optically thin material (Damm and Fedorov 2004); thus, Eq. (48) is applicable in the YSZ domains. The work of Murthy and Fedorov (2003) has shown that the radiative heat flux strongly affects the temperature distribution in thick electrolytes (i.e., electrolyte supported cells), while the effect of radiation is negligible for thin electrolytes (i.e., anode-supported cells).

If the material is optically thick, the radiative heat flux can be calculated by the Rosseland diffusion approximation and included into the $\vec{q}$ term of Eq. (47) (Murthy and Fedorov 2003). The term $\vec{q}$ takes into account both the conductive and radiative heat fluxes and is given by:

$$\vec{q} = -(k_s + k_{rad})\nabla T \tag{49}$$

where k_s is thermal conductivity of the solid and k_{rad} expressed by the Rosseland approximation is given by:

$$k_r = \frac{16 n_r^2 \sigma_B T^3}{3\beta_e} \tag{50}$$

where n_r is the refractive index of the medium, σ_B is Stefan–Boltzmann constant, and β_e is the spectrally averaged mean extinction coefficient of the medium.

Heat transfer in porous media The problem of modeling the heat transfer in the porous domains of SOFCs, which are composed of mixed solid and gas phases, is usually addressed employing a local thermal equilibrium (LTE) approach that locally assumes the same temperature for gas species and solid structure. The LTE assumption is very common in thermal modeling of SOFCs and allows to use only one energy conservation equation for both the phases in the computational domain of the porous medium (Andersson et al. 2013; Haberman and Young 2004; Ferrero et al. 2015). The conservation equation is given by:

$$\left(\rho C_{\mathrm{p}}\right)_{\mathrm{eff}}\frac{\partial T}{\partial t}+\rho_{\mathrm{g}}C_{\mathrm{pg}}\boldsymbol{u}\cdot\nabla T=\nabla\cdot\left(k_{\mathrm{eff}}\nabla T\right)+Q_{\mathrm{v}} \tag{51}$$

where the terms $\left(\rho C_{\mathrm{p}}\right)_{\mathrm{eff}}$ and k_{eff} are effective transport parameters, namely the energy stored per unit volume and the effective heat conduction flux, both obtained as volume averages of the quantities defined for the gas and solid phases. The effective properties are given by:

$$\left(\rho C_{\mathrm{p}}\right)_{\mathrm{eff}}=\varepsilon\rho_{\mathrm{g}}C_{\mathrm{pg}}+(1-\varepsilon)\rho_{\mathrm{s}}C_{\mathrm{ps}} \tag{52}$$

$$k_{\mathrm{eff}}=\varepsilon k_{\mathrm{g}}+(1-\varepsilon)k_{\mathrm{s}} \tag{53}$$

where the subscripts "g" and "s" stand for gas and solid.

The validity of the LTE approach has been discussed by Damm and Fedorov for hydrogen fueled SOFCs (Damm and Fedorov 2006) and subsequently by Zheng et al. (2013) who investigated the local thermal non-equilibrium (LTNE) effects in SOFCs electrodes in the presence of methane reforming and ammonia thermal cracking. Both studies indicates that LTNE effects within SOFC electrodes lead to insignificant local temperature differences between gas and solid phases of the order 10^{-2}–10^{-3} K; thus, the LTE assumption can be safely adopted in the thermal modeling of SOFCs.

The heat transfer by radiation is not included in Eq. (51), since SOFC electrodes are opaque to radiation and have a negligible radiative conductivity (Damm and Fedorov 2005). However, the radiative heat flux should be considered when defining the boundary conditions by using the same approach described for the heat transfer in fluid domains. In this case, surface-to-surface radiation is imposed on the boundary between electrode and gas channel.

The volumetric heat source term of Eq. (51) must include all the sources (or sinks) related to the phenomena that occur within the SOFC electrode in both the solid and gas phases. Heat generation is related to three different phenomena: (1) electrochemical reactions, (2) chemical reactions, and (3) Ohmic losses due to the resistance of the materials to the charge flow (i.e., Joule effect).

The heat generation due to the electrochemical reactions can be divided in reversible and irreversible; the first one account for the thermodynamic heat released by the ideal reactions and the second one takes into account the heat released for the activation of the charge-transfer reactions. These source terms are given by:

$$Q_{\mathrm{el,rev}}=-\left(\frac{|i_{\mathrm{v}}|}{nF}\right)T\Delta\bar{s} \tag{54}$$

$$Q_{\mathrm{el,irr}}=\eta_{\mathrm{act}}|i_{\mathrm{v}}| \tag{55}$$

where $\Delta\bar{s}$ is the molar entropy change of the electrochemical reactions, the term $(|i_v|/nF)$ is the molar volumetric flow of reacted molecules steaming from the Faraday's Law, and η_{act} is the activation overpotential (see Sect. 4). As previously stated, anode-supported cells models frequently assume the electrochemical reactions to be confined at the interface between the fuel electrode and the electrolyte. If this assumption is adopted, the electrochemical heat generation should be imposed as a boundary condition at the electrode/electrolyte border instead of being included in the source term of Eq. (51).

In typical SOFC systems, chemical reactions between the gas species occur in the anode, where gas streams typically containing H_2, H_2O, CO, CO_2, and CH_4 come in contact with the metal phase of the porous structure—usually nickel—which promotes the heterogeneous chemical reactions (see Sect. 5). The chemical reactions can be endothermic or exothermic, thus the chemical source term of Eq. (51) can be positive or negative depending on the reaction. The chemical heat source is given by:

$$Q_{\text{chem}} = -\sum_i \gamma_{si} r_i \Delta\bar{h}_i \tag{56}$$

where $\Delta\bar{h}_i$ is the molar enthalpy of reaction.

The ohmic losses are due to electronic and ionic resistivities of the solid structure of the electrode. Under operating conditions, SOFC electrodes are traversed by ionic and electronic currents—which depend on electrode morphology, temperature, and reactant distributions—that can be determined by using an electrochemical model of the cell (see Sect. 4). The heat released in the electrode volume due to the ohmic losses is calculated as in Eq. (48) by using the effective conductivity of the electronic/ionic phase in the porous media, whose expression is given in Eq. (81).

Finally, ohmic heating due to contact resistance between electrodes and interconnects should also be taken into account when defining the thermal boundary conditions.

$$-\boldsymbol{n} \cdot (-k_{\text{eff}} \nabla T) = Q_{\text{ohm,res}} \tag{57}$$

This type of resistance is usually expressed in terms of an area-specific resistance (i.e., $\Omega\ \text{cm}^2$) that depends on the contact method, the interface area between the materials and their resistivities (Wu et al. 2013). The heating source is given by:

$$Q_{\text{ohm,res}} = R_{\text{con}} \left|\vec{i}_b\right|^2 \tag{58}$$

where $\left|\vec{i}_b\right|$ is the absolute loss of the local current per unit surface that is crossing the boundary interface.

4 Electrochemical Modeling

The goal of an electrochemical SOFC model is to provide a mathematical formulation of the relation between the electrical variables of the fuel cell (i.e., current and voltage) and the thermo-fluidic and chemical ones (i.e., temperature and species partial pressures). In order to do this, it is necessary to implement in the model equations that give a suitable description of the electrochemical phenomena occurring in a fuel cell.

Before going into the details of the physics-based modeling, a brief introduction is given to highlight the main phenomena that an electrochemical model must address.

A SOFC is an electrochemical device that performs the direct conversion of the chemical energy of a fuel into electricity through redox reactions. The reactants (fuel and oxygen) are supplied in the gaseous form to the electrodes of the cell, where the electrochemical reactions take place, and an ion conductive layer—the electrolyte—ensures that the charged molecules produced in the redox processes can move between the electrodes. A potential difference arises between electrodes when reactants are supplied to them; if the electrodes are not electrically connected, this potential difference is exactly the electromotive force due to redox reactions and represents the maximum potential difference that the cell could achieve with these reactants. Instead, if the electrodes are connected through an external electrical circuit, the electrons move from an electrode to the other driven by the potential difference and irreversible phenomena connected to electrochemical reactions and charge transport occur and reduce the available potential difference.

A complete electrochemical model should encompass all these phenomena and give a mathematical description of the following: (1) generation of potential difference between electrodes, (2) electrochemical reactions, and (3) charge transport.

In the following sections, the description of the three aforementioned phenomena is given by presenting an overview of the approaches usually followed in the physical-based SOFC modeling.

Modeling the Equilibrium Potential The generation of a potential difference between the anode and cathode of a fuel cell depends on the redox reactions occurring at the electrodes. In general, the overall half-cell reactions consist in the oxidation of fuel molecules at the anode and the reduction of oxygen (or other oxidizing agents) at the cathode.

Typical fuels that are oxidized at the anode are hydrogen and carbon monoxide, but solid carbon, hydrogen sulfide, methane, and other higher hydrocarbons can participate directly to the electrochemical oxidation. In this chapter, the analysis will be limited to reactions involving H_2 and CO, as they are the electrochemical fuels in the vast majority of SOFC applications. The methane is frequently provided directly to the SOFC; however, it plays a role more as a reactant into the internal reforming reactions in which H_2 and CO are produced (see Sect. 5) rather than being the principal fuel in the electrochemical oxidation processes.

The half-cell oxidation reactions for H_2 and CO in SOFCs with oxygen-conductive electrolytes are given by:

$$H_2(g) + O^{2-}(el) \leftrightharpoons H_2O(g) + 2e^- \tag{59}$$

$$CO(g) + O^{2-}(el) \leftrightharpoons CO_2(g) + 2e^- \tag{60}$$

The oxygen reduction at cathode is given by:

$$O_2(g) + 4e^- \leftrightharpoons 2O^{2-}(el) \tag{61}$$

The reversible potential of the cell generated by the redox reactions—which is also called equilibrium, open-circuit, Nernst potential, or voltage—is the theoretical maximum potential difference that a fuel cell can produce between the electrodes for a given reactants composition. The reversible potential can be expressed as the difference between the equilibrium potentials of the reactions occurring at the anode and the cathode (Bagotsky 2005):

$$E_{\text{rev}} = E_{\text{eq},c} - E_{\text{eq},a} \tag{62}$$

The equilibrium potentials are functions of the Gibbs free energy of reaction, which depends on the temperature and activities of reactants and products. The equilibrium potential of the single electrode is given by:

$$E_{\text{eq}} = \frac{1}{n_e F}\left[\Delta \bar{g}_e^o + RTln\prod_k a_k^{v_k}\right] \tag{63}$$

where n_e is the number of electrons exchanged per molecule of fuel/oxidant in the electrode reaction, $\Delta \bar{g}_e^o$ is the molar standard-state free energy change of the reaction, a_k is the activity of species k, and v_k is the stoichiometric coefficient of the species (negative for reactants). In the case of gaseous reactants/products at low pressure—typical conditions of SOFC electrodes—the activity can be expressed as the ratio of the partial pressure of the gas over the standard pressure. For the coupled reactions (59)–(61) and (60)–(61), Eqs. (62) and (63) (84) result in the Nernst's formulation of the reversible potential:

$$E_{\text{rev},H_2-H_2O} = \frac{RT}{4F} ln\left(\frac{p_{O_2}^{\text{TPB}}}{p^o}\right) - \frac{1}{2F}\left[\Delta \bar{g}_{H_2-H_2O}^o + RTln\left(\frac{p_{H_2O}^{\text{TPB}}}{p_{H_2}^{\text{TPB}}}\right)\right] \tag{64}$$

$$E_{\text{rev},CO-CO_2} = \frac{RT}{4F} ln\left(\frac{p_{O_2}^{\text{TPB}}}{p^o}\right) - \frac{1}{2F}\left[\Delta \bar{g}_{CO-CO_2}^o + RTln\left(\frac{p_{CO_2}^{\text{TPB}}}{p_{CO}^{\text{TPB}}}\right)\right] \tag{65}$$

where the partial pressures are those of the species on the reacting surfaces, i.e., the TPB.

In most of the SOFCs models, the potentials given by Eqs. (64) or (65) are rearranged to show the species concentration in the bulk of the feeding gases:

$$E_{\mathrm{rev},\mathrm{H_2}-\mathrm{H_2O}} = -\frac{\Delta \bar{g}^{o}_{\mathrm{H_2}-\mathrm{H_2O}}}{2F} + \frac{RT}{2F} ln\left[\frac{p^{\mathrm{b}}_{\mathrm{H_2}}}{p^{\mathrm{b}}_{\mathrm{H_2O}}}\left(\frac{p^{\mathrm{b}}_{\mathrm{O_2}}}{p^{o}}\right)^{1/2}\right] - \eta_{\mathrm{conc},a} - \eta_{\mathrm{conc},c} \tag{66}$$

where the first two terms on the right side grouped together are referred to as reversible voltage under open-circuit conditions—usually named V_{oc}—and η_{conc} is the concentration overpotential due to the variation of the partial pressure of the species from the bulk of feeding streams to the reacting regions of the electrodes. The concentration overpotential is given by:

$$\eta_{\mathrm{conc}} = \frac{RT}{n_e F}\ln\left(\prod_k \frac{p_k^{b^{\nu_k}}}{p_k^{\mathrm{TPB}^{\nu_k}}}\right) \tag{67}$$

The difference in species concentration between the feeding flow and the reacting zone is usually attributed to the depletion of fuel/oxidizer due to the electrochemical reactions and to the mass transfer limitations in the electrodes that determine lower partial pressure of reactants in the TPB. Thus, the concentration overpotentials are frequently neglected at open-circuit, when electrochemical reactions do not occur. However, this is an oversimplification if gas streams contain components that can chemically react among themselves; in this case, the species concentrations also vary because of the chemical reactions even if the cell is at open-circuit.

A large part of SOFC models use Eq. (66) in combination with the activation and ohmic overpotentials to obtain the voltage of the cell:

$$V_{\mathrm{cell}} = V_{\mathrm{oc}} - \eta_{\mathrm{conc},a} - \eta_{\mathrm{conc},c} - \eta_{\mathrm{act},a} - \eta_{\mathrm{act},a} - \eta_{\mathrm{ohm}} \tag{68}$$

This is the standard expression of the cell polarization, usually adopted in the models to impose a constraint to the sum of the overpotentials of the cell (Fig. 3).

Given certain temperature and species distributions calculated from the thermo-fluidic models, the dependent variable of the polarization equation is the current density, which is given by the solution of Eq. (68). It is worth noting that the use of the Nernst's equation for the calculation of the reversible potential is not rigorously valid or applicable in all the models, unless proper assumptions are made. In particular, the Nernst's potential is a singular scalar value, whose calculation requires to evaluate the difference between the equilibrium potentials of anode and cathode; however, these two potentials are defined in different domains and the subtraction can be made if and only if each of them assumes a single scalar value. This is always true in 0-D models, but for higher dimension models the equilibrium potentials in general are not constant within the electrodes. Common assumptions adopted in 1-D and 2-D models impose the electrochemical reactions

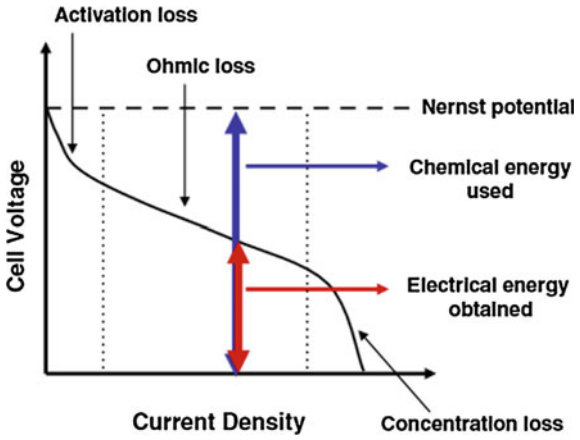

Fig. 3 Polarization curve. [Reprinted with permission from Kim et al. (2009)]

at the electrode/electrolyte interface and assume the electrodes as ideal electron conductors on which the electronic potential is constant (Ferrero et al. 2015; Ni 2009; Janardhanan and Deutschmann 2007). In this way, the TPBs are treated as lines on which the equilibrium potential varies with the position along the length of the electrode, and the Nernst potential can be calculated as the difference between the anodic and cathodic equilibrium potentials at each position of the electrode length. Another further assumption can be made by considering the equilibrium potential of the cathode as a constant, because in SOFC applications the composition of the air electrode mixture is less variable than the anodic one during the operations.

The use of Nernst's equation has no meaning in 3-D models or 2-D models where electrochemical reactions are imposed in the volume instead of being assumed at the electrolyte/electrode interface. In this case, a more general modeling approach based on the implementation of equations which contain the electronic and ionic potentials of the cell as dependent variables should be used. With this approach, it is not necessary to calculate a reversible potential to be introduced in a polarization equation, but it is sufficient to calculate the local equilibrium potential with Eq. (66) or by using the potential expression dependent on oxygen partial pressure in the gas mixture at equilibrium, as shown later in the case of multi-fuel mixtures. The current density produced in the cell can be then calculated as a function of the difference between electronic, ionic, and equilibrium potentials in the TPBs regions by implementing a Butler–Volmer equation for the charge-transfer reactions, as will be shown in the next pages, and the transport of charge is the result of the gradients of the potentials. In the general approach based on the potentials, the voltage of the cell is imposed on the surface of one of the electrodes as a boundary condition for the electrical potential, while on the surface of the other the ground potential (i.e., zero potential) can be assumed.

Some considerations have to be spent in the case of multi-fuel mixtures. In principle, when two or more different electrochemical reactants (i.e., H_2 and CO)

are present at the anode at the same time, each oxidation reaction has a different value of equilibrium potential, and thus, it seems not possible to define a unique value of reversible potential. However, it is possible to demonstrate that, under the assumption of having the fuel mixture in equilibrium conditions on the TPB surfaces of the electrode, the equilibrium potential is the same for all the fuels, and consequently, it is possible to define unambiguously the reversible potential of the cell.

When the chemical equilibrium of the gaseous species within the electrode is assumed, the Nernst's voltage can be also re-written in terms of the oxygen partial pressures in the anode and cathode TPBs:

$$E_{\text{rev}} = \frac{RT}{4F} ln \left(\frac{p_{O_2}^{\text{TPB,cat}}}{p_{O_2}^{\text{TPB,an}}} \right) \tag{69}$$

where the partial pressure of oxygen at the anode is directly evaluated by calculating the equilibrium composition of the gas mixture. Expression (69) is useful to evaluate the ideal reversible potential of multi-fuel mixtures inside the anode just from the equilibrium composition of the fuel mixture.

It is worth noting that the equality between the equilibrium potentials of different reactions in multi-fuel mixtures is not valid when the gas mixture within the anode is far from equilibrium. If we consider anode-supported SOFCs with Ni/YSZ anodes, the equilibrium assumption can be considered applicable because the fuel gas has to cross a large volume of electrode before reaching the TPB, and thus, it has a sufficient contact time with the nickel catalyst that allow gas-shift and other reactions to reach the equilibrium. However, the gas equilibrium assumption has to be carefully verified case by case before applying it into a model.

If the gas mixture is not in equilibrium, it is not possible to define a single value of equilibrium potential within the electrode and both the Nernst- and potentials-based approach are not applicable. In this case, an elementary mass-action formulation based on the modeling of the rates of the single charge-transfer reactions is needed (Goodwin et al. 2009). As will be shown in the next section, with this approach, it is possible to avoid the calculation of the equilibrium potentials because the current generated by the electrochemical reactions is computed directly from the rates of the single charge-transfer reactions and the use of Butler–Volmer formalism is not required.

Electrochemical Reactions Modeling The electrochemical reactions can occur only where electron conductive, ion conductive, and gas phase coexist. The simultaneous presence of the three phases allows the conduction of electrons, the migration of ions, and the transport of gas molecules to/from the reaction sites. As stated before, these are the TPB regions of the electrodes.

The mere presence of the TPB is not sufficient to ensure the electrochemical reactions to happen, but the TPB must be connected to the rest of the structure. If either the electronic, ionic, or pore network is interrupted or badly interconnected,

the electrochemical reactions cannot take place properly because electrons, ions, or gaseous reactants/products cannot reach or leave the TPB surfaces. Most of the electrode materials are predominantly electronic conductors (e.g., Ni metal and La–Sr–Mn oxides), and when these materials are used, the TPB is limited to the contact region between the electrode and the electrolyte. In particular, the commonly used anode Ni–YSZ cermets have a TPB extension that several studies have estimated in the order of 5–20 μm (Cai et al. 2011; Zhu and Kee 2008). The TPB length of SOFC cathodes can be typically higher, when mixed ionic and electronic conductors are used as cathode materials.

The reaction mechanisms that occur on the TPB consist of complex chains of intertwined physiochemical phenomena, which include adsorption/desorption of gas molecules on/from the electrode surface, dissociation, surface transport and solid-state diffusion of adsorbed species, and charge-transfer reactions. The study of electrochemical reaction mechanisms of SOFC electrodes has been addressed by countless works, and it is out of the scope of this chapter, a thorough review of the literature pertaining these mechanisms has been presented by Hanna et al. (2014) and Li et al. (2010).

The problem of modeling the electrochemical reaction mechanisms is usually addressed by following two different approaches: (1) by assuming a charge-transfer step to be the rate-determining step of the entire reaction mechanism and using Butler–Volmer expressions for the calculation of the current electrochemically generated in SOFC (Noren and Hoffman 2005) or (2) by using fundamental mass-action kinetics to describe each elementary reaction of the entire mechanism and calculating the electrochemical current from the rates of the elementary charge-transfer reactions (Goodwin et al. 2009).

In the following paragraphs, these two different modeling approaches are described.

In both approaches, it is necessary to define what the elementary steps of the reactions are, but in the first one, the total rate of the electrochemical reaction is assumed to be controlled only by the transfer of the electric charge at the TPB and not by the transport of the species. Most of the SOFC models adopt this approach and use the Butler–Volmer equation either combined with a polarization equation that couples the reversible cell potential—usually calculated by the Nernst's equation—with the voltage losses (i.e., overpotentials) related to the irreversible phenomena, namely the activation; ohmic and concentration overpotentials are expressed as a function of the electric, ionic, and equilibrium potentials. Some authors have also adopted a mixed approach where the description of elementary charge-transfer reactions through mass-action kinetics is introduced into the Butler–Volmer formulation by adopting simplifying assumptions (Zhu et al. 2005; Menon et al. 2013).

When the global electrochemical reaction is assumed to be controlled by a charge-transfer step, the Butler–Volmer equation can be used to calculate the net current density generated in the electrode by the reaction (Bagotsky 2005):

$$i = i_0 \left[\exp\left(\alpha_f \frac{n_{BV} F \eta_{act}}{RT} \right) - \exp\left(-\alpha_b \frac{n_{BV} F \eta_{act}}{RT} \right) \right] \tag{70}$$

where i_0 is the exchange current density of the electrode reaction, α_f and α_b are symmetry parameters of forward and backward reactions, η_{act} is the activation overpotential of the reaction, and n_{BV} is the number of electrons transferred in the charge-transfer step. It is worth noting that only if the electrochemistry is represented with a single, global charge-transfer process that corresponds with the half-cell reaction (Shi et al. 2011), then n_{BV} is the number of electrons transferred in the half-cell reaction.

If the Bulter–Volmer equation is describing a global charge-transfer reaction, the coefficients α_f and α_b have no constraints, while for elementary reactions—in which only one electron is transferred—these factors take on values between 0 and 1 and their sum is constrained to 1 (Goodwin et al. 2009).

The activation overpotential arises because the electric charge cannot move directly between the ionic and electronic conductive phases of a cell. Both the phases have free charge carriers and are globally neutral, however an excess charge is distributed on their surfaces. Therefore, at the interface between the phases—the TPB—an electric double layer is formed, with the charged surfaces behaving as the plates of a capacitor. During the charge-transfer reaction, the electrons are transferred across the double layer moving against the potential difference existing between the ionic and electronic phases. When the net current crossing the double layer is zero, the potential difference between the phases is equal to the equilibrium potential of the electrode, while if a potential difference higher than the equilibrium is needed to allow a non-zero net current to exist. The activation overpotential measures the disequilibrium between the potential difference in the phases and the equilibrium potential:

$$\eta_{act} = \phi_e - \phi_i - E_{eq} \tag{71}$$

where ϕ_e is the electronic potential of the electrode, ϕ_i is the ionic potential and E_{eq} is the equilibrium potential of the electrode that can be expressed by using Eq. (63).

In most of models that use a Butler–Volmer approach, the activation overpotential is related to the current density by Eq. (71) that is coupled to the polarization Eq. (68) to solve the electrochemical problem and obtain the current density distribution without explicitly introduce the ionic and electronic potentials in the equations (Chan et al. 2001; Ni et al. 2007; Ferrero et al. 2015). However, for the distributed charge-transfer modeling in 2-D and 3-D models, the electronic and ionic potentials are frequently used as dependent variables instead of the current density; in this case, the activation overpotential is expressed by using Eq. (71) and the Butler–Volmer equation is coupled with the charge transport equations to define the current density distribution within the electrodes (Zhu et al. 2005; Klein et al. 2007; Shi et al. 2007; Andersson et al. 2012).

The exchange current density provides a quantitative measure of the electrocatalytic activity of the electrode for a certain electrochemical reaction. Its value depends on the charge-transfer kinetics, temperature, partial pressures, and electrode microstructure. The dependency of i_0 on so many parameters makes it difficult to define it without the use of semi-empirical relations. In most of the SOFC literature, the exchange current density is expressed as the product of temperature-dependent terms, written in Arrhenius form, and pressure-dependent terms (Costamagna and Honegger 1998; Hosoi et al. 2015):

$$i_0 = \gamma \cdot \exp\left(-\frac{E_{\text{act}}}{RT}\right) \prod_k \left(\frac{p_k}{p_{k,\text{ref}}}\right)^{e_k} \tag{72}$$

where p_k is the partial pressure of the k species involved in the electrochemical reaction as reactant or product and $p_{k,\text{ref}}$ is a reference pressure for the k species. E_{act} is the activation energy of the electrode reaction, which depends on reaction and materials, e_k is a dimensionless exponent and γ is a pre-exponential parameter dependent on electrode materials and microstructure, and in some cases also on the temperature (Leonide 2010). The values of γ and e_k are widely scattered in the literature.

Equation (72) is a semi-empirical relation in which the parameter γ is usually determined by fitting experimental data. Theoretical expressions of the exchange current density have been derived by Hosoi et al. (2015) and Zhu et al. (2005) from the study of reaction mechanisms. In these works, the current density is expressed as a function of rates and equilibrium constants of the elementary reactions that are assumed to compose the entire reaction mechanism. The theoretical formulation of the exchange current density allows to describe its dependency on the partial pressures in a physically based way; however, the high number of constant dependent on reactions and materials makes it necessary to use empirical data for a quantitative evaluation of i_0.

It is worth noting that the current density evaluated by Eq. (70) is expressed per unit of electrochemically active area of the electrode; thus, in order to obtain the volumetric current generated in the electrode, namely i_v. The current density has to be multiplied by the active electrode area per unit volume (Costamagna et al. 1998):

$$i_\text{v} = A_\text{v} i \tag{73}$$

The use of Butler–Volmer equation is consistent when the charge transfer is the rate-determining step of the electrochemical reaction, and its application requires the definition of an equilibrium potential within the electrode; however, if the gas mixture is not in equilibrium, it is not possible to define properly the equilibrium potential and the Butler–Volmer is not applicable. In this case, the current density generated by the electrochemical reaction can be calculated by using an elementary mass-action formulation of the rates of the elementary charge-transfer reactions (Goodwin et al. 2009).

In general, a charge-transfer reaction can be written as:

$$A^a + B^b \leftrightharpoons C^c + D^d + \upsilon_e e^- . \tag{74}$$

where A, B, C, and D are the species having charge a, b, c, and d that are involved in the transfer of υ_e electrons. For an elementary charge-transfer reaction, the coefficient υ_e assumes the value of +1 for the forward (i.e., anodic) reaction—which "produces" electrons—and −1 for the backward (i.e., cathodic) reaction. The net rate of the reaction is given by the difference in the forward and backward rates of the charge-transfer reaction, which can be written as follows:

$$q_{i,\mathrm{f}} = k_{\mathrm{f}}(T) \prod_{i,r} a_i \exp\left(\frac{\beta_{\mathrm{f}} \mathrm{FE}_{\mathrm{el}}}{RT}\right) \tag{75}$$

$$q_{i,\mathrm{b}} = k_{\mathrm{b}}(T) \prod_{i,p} a_i \exp\left(-\frac{\beta_{\mathrm{b}} \mathrm{FE}_{\mathrm{el}}}{RT}\right) \tag{76}$$

where the rate constants k can be expressed in the Arrhenius form, a_i are the activities either of the reactants in the case of the forward reaction or of the products for the backward one. The coefficient β_{f} and β_{b} are the symmetry coefficients, which range between 0 and 1 and are constrained to have sum equal to one. E_{el} is the electrode potential, which is given by:

$$E_{\mathrm{el}} = \phi_e - \phi_i \tag{77}$$

The current generated for unit of TPB length is given by:

$$i_{\mathrm{TPB}} = F \sum_i \left(q_{i,\mathrm{f}} - q_{i,\mathrm{b}}\right) \tag{78}$$

where the summation includes all the charge-transfer reactions. The volumetric current density is related to i_{TPB} by the volume-specific TPB length (Janardhanan et al. 2008):

$$i_{\mathrm{v}} = \lambda_{\mathrm{TPB}} i_{\mathrm{TPB}} \tag{79}$$

With this approach, it is possible to calculate the current generated by the electrochemical reactions by avoiding the Butler–Volmer formulation.

Charge transport and conservation In an SOFC stack, the charge transport takes place in the solid phases—ionic and electronic—of cells and components.

Both the ionic and the electronic conductive materials exert a resistance to the charge flow and the movement of charges is driven by the potential difference existing between the electrodes of the cells. The charge flux is referred to as the current density, which is given by the Ohm's Law:

$$i_{i/e} = -\sigma_{i/e} \nabla \phi_{i/e} \tag{80}$$

where $\nabla \phi_{i/e}$ is the gradient of the ionic/electronic potential that drives the charge flow and $\sigma_{i/e}$ is the conductivity of the material. In the case of the impervious solids (i.e., electrolyte, interconnects, and current collectors), the conductivity is that of the pure material, while in the porous electrodes, an effective conductivity must be calculated in order to take into account the presence of pores and electron-conductive phase. The effective conductivity can be calculated by using a statistical approach in which the porous electrode is assumed as system of packed spherical particles (Nam and Jeon 2006). The effective conductivity is given by:

$$\sigma_{i/e}^{\text{eff}} = \sigma_{i/e} \left[(1 - \varepsilon) f_{i/e} P_{i/e} \right]^k \tag{81}$$

where $f_{i/e}$ is the volume fraction of the ionic/electronic phase in the electrode and $P_{i/e}$ is the percolation probability. The exponent k, generally larger than 1, depends on the distribution of the conductive phase in the electrode.

The conservation equation must be applied in the model to enforce the conservation of charge:

$$\frac{\delta \chi_{e/i}}{\delta t} + \nabla \cdot i_{e/i} = \psi_{i/e} \tag{82}$$

where $\chi_{e/i}$ is the volumetric charge density and $\psi_{i/e}$ is the volumetric charge source. The term $\psi_{i/e}$ is different from zero only when the charge-transfer reactions are assumed to take place in the volume of the electrode. In this case, the charge is transferred from the ionic to the electronic phase of the electrodes in the TPB volume of the electrodes; the variation of ionic and electronic currents is given by:

$$\psi_{i/e} = \pm i_{\text{v}} \tag{83}$$

where i_{v} is the current that is transferred at the TPB, which is calculated from Eqs. (73) or (79).

When the electrochemical reactions are imposed at the interface between electrode and electrolyte, the volumetric charge source is null, and the continuity between the ionic and electronic current is imposed on the boundary.

In SOFC models, the charge transport in the electronic conductive materials is usually neglected by assuming them as ideal conductors (i.e., infinite conductivity) and only the transport of ions in the electrolyte is taken into account. Also, the ions transport is frequently assumed to be one-dimensional and normal to the electrolyte/electrode interfaces. This assumption is valid for thin electrolytes and allows to express the potential drop due to ion transport as the difference between the potentials at electrode/electrolyte interfaces:

$$\eta_{\text{ohm}} = \phi_{i,\text{an}} - \phi_{i,\text{cat}} \tag{84}$$

Equation (71) involves the electric/ionic potentials as dependent variables, which are put in relation by Butler–Volmer (70) or elementary rate Eqs. (75) and (76) imposed on the TPB boundary or volume. On the external surface of the electrodes or on the current-collecting plates in the case of a stack, where only the electrical potential is defined because the ionic phase is not present, a boundary condition is needed in order to solve the charge-conservation equation. The cell (or stack) voltage is usually imposed on one of the electrode (or current collector) surfaces, while on the other the ground (i.e., zero) potential is fixed.

Another possible approach is to impose the ground potential on one of the electric boundaries and fix the total current value on the other by imposing a constraint to the integral of the current density:

$$\int_{\partial\Omega} i \cdot \vec{n} \mathrm{d}S = I_{\text{tot}} \tag{85}$$

With this approach, the input of the electrical model is the current, while the voltage of the SOFC cell/stack can be calculated from the difference between the potentials on the two electric boundaries.

5 Modeling the Heterogeneous Chemistry in SOFCs

Chemical reactions can occur within the fuel stream at the typical operating conditions of SOFCs. In particular, when fuels other than hydrogen are fed to the cells, the operating temperatures are sufficient to promote both homogeneous and heterogeneous reactions between the fuel components.

If we consider the typical SOFC mixtures—which contain H_2, H_2O, CO, CO_2 and CH_4—and operating conditions, the reactions that occur within the gas phase are very slow when compared to the heterogeneous ones; thus, the homogeneous chemistry can be safely neglected in the anode domains (Zhu et al. 2005). In particular, when the fuel mixture comes in contact with the porous structure of the anode, typically made by a Ni/YSZ cermet, the heterogeneous reactions are promoted by the presence of the nickel that acts as a catalyst for the reactions, such as methane reforming and gas shifting. However, homogeneous reactions can play a non-negligible role in non-catalytic SOFC regions when dry natural gas (Walters et al. 2003) or higher hydrocarbons are fed to the cells—especially at very high temperatures ($T > 800$ °C)—or when partial oxidation conditions are reached (Gupta et al. 2006) due to the presence of oxygen or air into the fuel stream.

This chapter will focus on the modeling of the heterogeneous reactions in SOFC anodes. Modeling the reactions means to find a suitable mathematical description of the physics that allows to calculate the rates of the reactions. In particular, rates are

necessary to interface the chemical model with the thermal and fluidic ones through the source terms of Eqs. (6) and (56).

The problem of describing the heterogeneous reaction rates has been addressed in the SOFC literature in two different ways: by using global expressions for the calculation of an overall reaction rate or through detailed kinetic models that include intermediate reaction steps. Both the approaches are based on the mean-field approximation, which describes the surface state with average quantities and neglects the non-uniformity of the catalytic surfaces.

Global reaction mechanism Two different approaches can be adopted when modeling the chemistry by using global rate expressions: one is based on the assumption that the reaction is controlled by kinetics and the other assumes that the reaction rate is limited by the equilibrium.

The first approach is based on modeling each reaction in a single step whose rate can be generally expressed by a kinetic power law expression:

$$r_{\text{react}} = \gamma_r \prod_i p_i^m \exp\left(-\frac{E_a}{RT}\right) \tag{86}$$

where γ_r and reaction orders m of the i species participating to the reaction are derived from the fitting of experimental data. Alternatively, to power law models, Langmuir–Hinshelwood type models are used to describe the kinetics.

With the second approach, the reaction velocity is expressed through an equilibrium-limited rate expression defined by:

$$r_{\text{react}} = r_{\text{f}}\left(1 - \frac{\prod p_{\text{products}}^{\nu}}{\prod p_{\text{reactants}}^{\nu}}\frac{1}{K_{\text{r}}}\right) \tag{87}$$

where ν is the stoichiometric coefficient of the gaseous species, K_{r} is the equilibrium constant of the reaction, and r_{f} is the rate of the forward reaction, usually given by a power law expression. It is worth noting that the rate expressed by Eq. (87) goes to zero when the equilibrium composition is reached.

The applicability of the equilibrium rather than the kinetic approach strictly depends on the reaction and on the complexity of the model. In general, if a lumped 0-D model is used for the cell, the equilibrium of the reactions can be safely assumed, while if a multidimensional model is adopted, then it is more appropriate to apply a kinetic description of the reaction for the calculation of local rates.

The approaches described by Eqs. (86) and (87) are valid for any reaction; however, their application requires to fit the kinetic expressions to experimental data measured under reaction conditions that are relevant for the model. Experimental data are available in the literature for the most common reactions and cell materials; however if the model has to include particular reactions, conditions, or materials, it is necessary to build specific experimental data sets in order to characterize the reactions and describe the catalytic activity of materials with respect to the investigated reactions.

The most common reactions included in SOFC models are the heterogeneous methane steam reforming (STR) and water–gas shift (WGS) reactions within Ni/YSZ anodes:

$$CH_4 + H_2O \leftrightharpoons CO + 3H_2 \tag{88}$$

$$CO + H_2O \leftrightharpoons CO_2 + H_2 \tag{89}$$

When these reactions are modeled using a global-mechanism approximation, the kinetic approach is usually adopted for the steam reforming reaction (88), while the water–gas shift (89) is frequently described under the equilibrium assumption. The kinetic expressions used for the steam reforming reactions are commonly derived from experimental studies either over commercial nickel-based catalysts (Xu and Froment 1989; Hou and Hughes 2001) or directly on Ni/YSZ anodes (Drescher et al. 1998; Achenbach and Riensche 1994; Ahmed and Foger 2000; Lee et al. 1990; Belyaev et al. 1995; Dicks et al. 2000). In the study of Nagel et al. (2008) different steam reforming models given by power law; Langmuir–Hinshelwood and equilibrium expressions have been compared showing the effect of the STR kinetics on the temperature distribution in the cell.

In the work of Sanchez et al. (2008), the equilibrium and kinetics approaches have been compared for both reactions (88) and (89). The work highlights that the rates of reactions are controlled either by kinetics or equilibrium depending on the local conditions of the cell, thus the choice between one approach and the other is strictly connected to the peculiarities of the modeled system and cannot be assumed a priori.

Besides the STR and WGS, other reactions frequently included in SOFC models by using global kinetics expressions are as follows: dry reforming ($CH_4 + CO_2 \leftrightharpoons 2CO + 2H_2$), methanation ($CH_4 + 2H_2O \leftrightharpoons CO_2 + 4H_2$), Boudouard ($2CO \leftrightharpoons CO_2 + C$), and methane cracking ($CH_4 \leftrightharpoons C + 2H_2$) (Wang et al. 2011b; Ni 2013).

It is worth noting that the equations introduced in this section for the calculation of an overall reaction rate do not include neither the concentrations of intermediate surface species on the anodic structure nor explicit information on the microstructure of the electrode, even if they are describing heterogeneous kinetics.

Detailed surface reaction kinetics Alternatively to the global rate expressions, the problem of modeling the heterogeneous chemistry can be addressed by using a mass-action formulation of the kinetics of the elementary reaction steps.

The principle is analogous to that showed when modeling the charge transfer with the mass-action formula instead of approximating the reaction with a global mechanism; a multi-step mechanism is developed and a rate is calculated for each step of the reaction.

The total molar rate of the i-th reaction step is given by the difference between forward and backward rates of reaction:

$$r_{\text{react},i} = k_{\text{f}i} \prod_{k=1}^{K} [X_k]^{\nu'_{ki}} - k_{\text{r}i} \prod_{k=1}^{K} [X_k]^{\nu''_{ki}} \tag{90}$$

where $k_{\text{f}i}$ and $k_{\text{r}i}$ are the rate constants of the reaction, K is the total number of species—gaseous and adsorbed on the surface—involved in the reaction step, $[X_k]$ is the concentration of the k species and the exponents ν'_{ki} and ν''_{ki} are the stoichiometric coefficients of reactants and products. The concentration of the k species is expressed either as molar volumetric (mol/m^3) for the gas-phase species or as molar superficial (mol/m^2) for the surface species.

If Eq. (90) is applied to all the reaction steps involving the k species, the resulting net molar rate is given by:

$$\dot{s}_k = \sum_{i=1}^{K_{\text{r}}} \left[\left(\nu''_{ki} - \nu'_{ki} \right) k_i \prod_{k=1}^{K_{\text{g}}+K_{\text{s}}} [X]_k^{\nu'_{ki}} \right] \tag{91}$$

In Eq. (91), K_{r} is the total number of reaction steps, K_{g} is the number of gas-phase species in the i-th step, and K_{s} is that of the surface species. The surface molar concentration can be expressed as a function of the surface coverage of the species:

$$[X_k] = \frac{\theta_k \Gamma}{\sigma_k} \tag{92}$$

where θ_k is the surface coverage of the k species, σ_k is the coordination number (i.e., the number of source sites that are occupied by species k), and Γ is the total surface site density.

The rate constants are expressed in Arrhenius form and can be also dependent on the surface coverage of adsorbed species:

$$k_i = A_i T^{\beta_i} exp\left(-\frac{E_{ai}}{RT} \right) \prod_{k=1}^{K_{\text{s}}} \theta_k^{\mu_{ki}} exp\left(-\frac{\in_{ki} \theta_k}{RT} \right) \tag{93}$$

where μ_{ki} and $\in_{ki}$ are parameters for modeling the coverage dependence. When the elementary step is an adsorption reaction of a gas-phase species on the catalyst surface, the rate constant is given by:

$$k_i = \frac{\gamma_{0i}}{(\Gamma)^m} \sqrt{\frac{RT}{2\pi M_{\text{g}}}} \tag{94}$$

where ς_i is the sticking coefficient of the reaction (i.e., a measure of the probability that the adsorption reaction takes place when the molecule collide with the surface, its value lies between 0 and 1), m is the sum of the stoichiometric coefficients of the reactants, and M_{g} is the molecular weight of the gas-phase species adsorbed.

When Eq. (91) is solved for all the k species in combination with the fluidic, thermal, and electrochemical equations, the surface coverages are included in the dependent variables and must be determined as a part of the solutions.

The surface coverage of a species depends on the position, because the local temperature and gas species concentrations vary within the electrode. However, the mean-field approximation ensures that the surface species do not interact laterally; thus, the surface coverage in a point of the surface is not influenced by the coverages in the neighboring positions of the computational domains and the time-dependent variation of θ_k can be written as follows:

$$\frac{\partial \theta_k}{\partial t} = \frac{\sigma_k \dot{s}_k}{\Gamma} \tag{95}$$

Equation (95) has to be imposed for all the surface coverages, and the solution of the resulting system of differential equations provides the values of θ_k. However, the times scales of the surface reactions are several order magnitudes lower than those of the variation of temperature and gas-species concentrations. Therefore, the steady state approximation can be applied and the system of Eq. (95) reduces to a set of algebraic equations in which the net molar rates of the surface species are imposed to be equal to zero.

The approach based on elementary reaction mechanisms has a broader validity with respect global mechanism approaches since it can include all the possible chemical reactions occurring within the porous anode. Moreover, the mass-action formulation has a general validity can be applied also to homogeneous chemistry.

A multi-step reaction mechanism for the internal reforming of CH_4–CO–CO_2–H_2–H_2O–O_2 mixtures has been developed and validated over Ni/YSZ cermets by Hecht et al. (2005). The mechanism, which consists of 42-reaction steps that involve 6 gas-phase species and 12 surface species, has been recently applied in the modeling and validation of the heterogeneous chemistry in tubular SOFCs fed by biogas (Santarelli et al. 2013), and its comparison with a global kinetic approach is reported by Hoffman et al. (2009). The multi-step mechanism predicts slower methane conversion with respect to the global kinetic approximation (Hoffman et al. 2009) and shows that thermodynamic equilibrium conditions are not fully achieved inside the anode of a tubular fuel cell, consistently with the experimental observations (Santarelli et al. 2013).

6 SOFC Modeling: Examples of a Multidimensional Approach

The modeling approach presented in this chapter provides a mathematical description of the physical phenomena occurring in SOFCs from a macroscopic point of view.

In the literature, macroscopic SOFC models have been developed from 0-D to 3-D depending on the model objectives. The following sections provide some representative examples of the multidimensional approaches followed in the physically based SOFC modeling.

0-D models Zero-dimensional models are box models that allow the calculation of scalar variables, returning results independent from a spatial description of the physics. These models are typically used to simulate the polarization of an SOFC and analyze the cell performance with the variation of operating conditions (e.g., mean cell temperature and pressure) or geometrical parameters (e.g., electrode thickness).

An example is the zero-dimensional SOFC electrochemical model presented by Chan et al. (2001), which describes the polarization characteristic of a cell operating with H_2/H_2O mixtures by calculating the cell voltage using Eq. (68). The model takes into account the diffusion in porous electrodes by integrating diffusive Fick's flows along the thickness of the electrodes and describes the activation overpotential by the Butler–Volmer Eq. (70). Sensitivity analyses are performed with the model to investigate the effect of electrodes' thickness on polarization curve and cell overpotentials (Fig. 4).

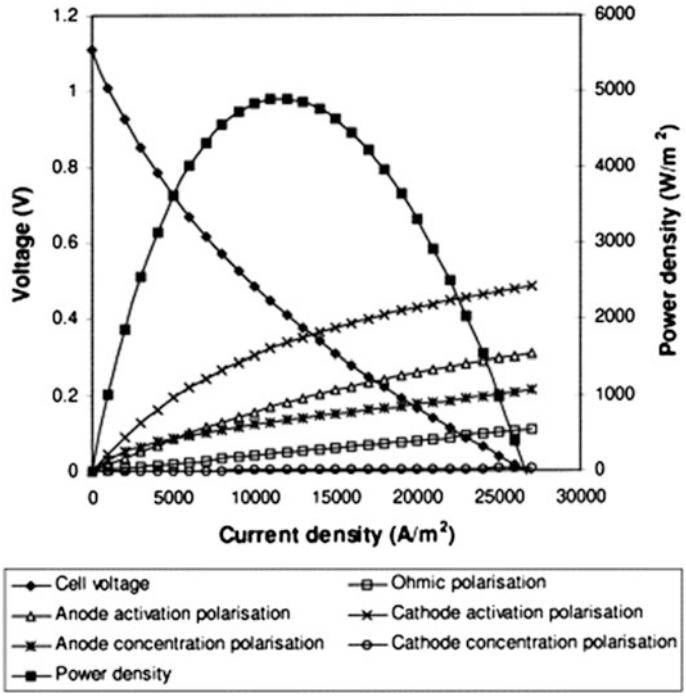

Fig. 4 Cell voltage, polarization losses, and power density for an anode-supported SOFC (anode thickness 750 μm) operating at 800 °C. [Reprinted with permission from Chan et al. (2001)]

1-D models One-dimensional models give a spatial-dependent description of the phenomena. Typically, 1-D models are used to describe the evolution of thermo-electrochemical variables within the cell by considering one dominant geometrical dimension—usually the gas flow direction—and simplifying the equations in the other directions.

A one-dimensional model for the simulation of biogas reforming in a tubular, anode-supported SOFC with Ni/YSZ anode has been presented by Santarelli et al. (2013). The model divides the SOFC in series of elements along the axial direction of the cell and each of them is solved unidimensionally along the radial coordinate by assuming that diffusive transport is dominant over convection. The reforming process is modeled following an elementary kinetics approach by including in the model the multi-step reaction mechanisms developed by Hecht et al. (2005). The anode volume is approximated by a surface located at the channel/electrolyte interface, and the model resolves the species conservation Eq. (3) with chemical source terms calculated from the kinetic model and electrochemical sources evaluated by imposing the current density on the anode boundary and evaluating the species molar fluxes by Faraday's law (7). The model evaluates the evolution of mole fractions of chemical species along the fuel channel for a given temperature and current (Fig. 5). Model results are close to gas compositions obtained from experimental measurements and indicate that thermodynamic equilibrium is not completely achieved within the anode channel, as at the outlet composition is different from that predicted by chemical equilibrium.

2-D models Two-dimensional models are generally used for the simulation of cells and SRUs. Cell models of tubular SOFCs can be implemented by taking advantage of the axis-symmetric geometry, while planar SOFC models require the selection of a 2-D section representative of the entire cell/SRU, which is typically a cross section parallel to gas flow.

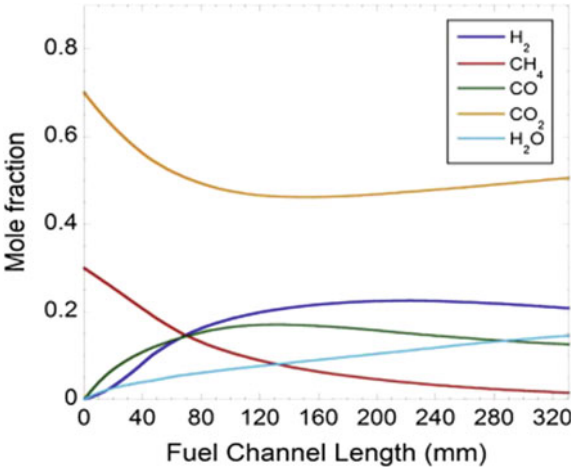

Fig. 5 Simulated mole-fraction profiles of chemical species along the fuel channel with CO_2/biogas ratio of 1, at 800 °C and 50 % of fuel utilization. [Reprinted with permission from Santarelli et al. (2013)]

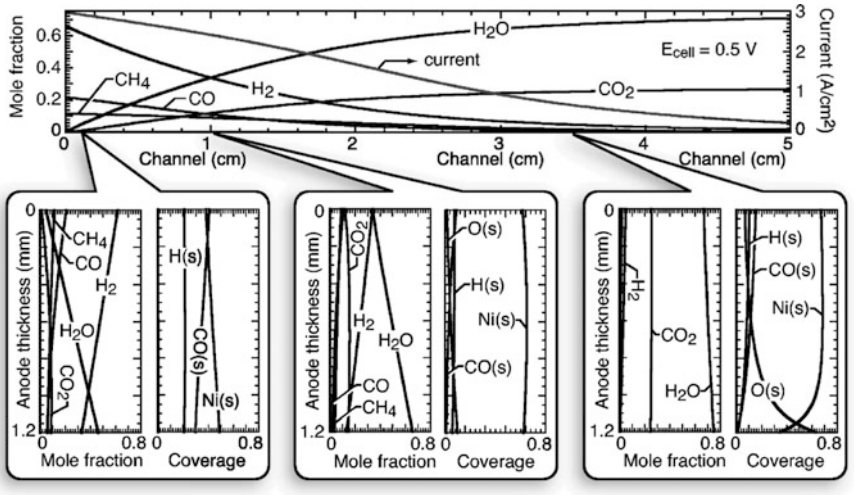

Fig. 6 Simulated distribution of species and current density for a fuel mixture of 66 % H_2, 22 % CO, and 12 % CH_4 entering the anode channel. Cell is operating at constant temperature (800 °C) and atmospheric pressure. The *upper panel* shows mole fractions and current density as functions of distance along the channel length. *Lower panels* show mole fractions and surface coverages through the thickness of the porous anode at different positions along the channel. [Reprinted with permission from Zhu et al. (2005)]

An example of 2-D model that encompasses both the electrochemical and chemical phenomena occurring in an SOFC is that developed by Zhu et al. (2005). The model describes a planar, anode-supported SOFC operating with carbon/hydrogen mixtures with co-flowing channels. A steady plug-flow model is applied to describe the channel flows, and the DGM model (29) is used to describe the diffusion in porous electrodes. Electrochemistry is implemented by considering Nernst (64) and Butler–Volmer Eqs. (70) for the hydrogen oxidation reaction, while the heterogeneous chemistry is described by implementing the elementary kinetics of the reaction mechanism assumed for hydrogen/carbon mixtures over Ni/YSZ. The model predicts the current–voltage performance of the cell and the species distribution in the channels and within the anode structure (Fig. 6).

3-D models Three-dimensional models are generally used for the simulation at full-stack or SRU level to accurately describe fluidic and thermal fields on complex geometries.

An example is the 3-D model developed by Qu et al. (2011). The model describes an anode-supported planar SOFC with corrugated bipolar plates acting both as gas channels and current collectors (Fig. 7).

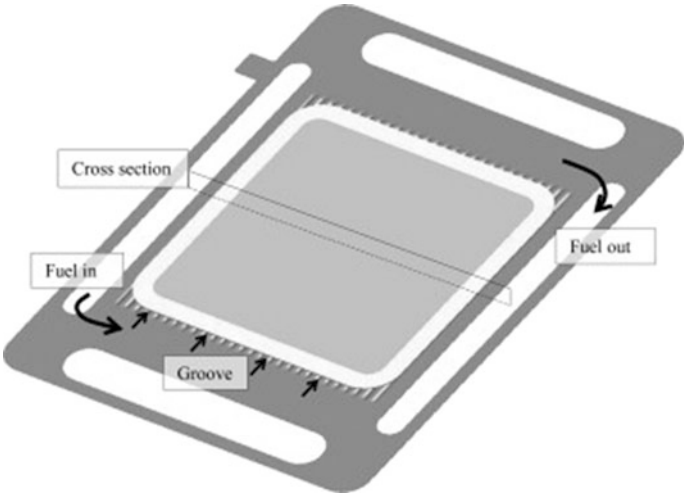

Fig. 7 Schematic drawing of the fuel flow and configuration of the modeled SOFC. [Reprinted with permission from Qu et al. (2011)]

The model applies the Navier–Stokes equations in the fluidic domains and describes the diffusion by using the SMM model (15). Heat transfer by conduction and convection is considered in the model, and the electrochemistry is described by applying the polarization Eq. (68) in which Nernst (64) and Butler–Volmer equations (70) are used to describe reversible voltage and activation overpotentials. The conservation of mass, momentum, energy, and species are solved together with the electrochemical equations, and the distributions of temperature, flow velocity, pressure, and species concentrations through the cell structure and gas channels are obtained.

The model is applied to study the current distribution in the SRU and results indicate that quite uniform distributions of current density over the active cell area can be achieved with the investigated geometry. The results also indicate that the geometry of cathode gas channel has a non-negligible effect on the oxygen distribution and thus on the overall cell performance (Fig. 8).

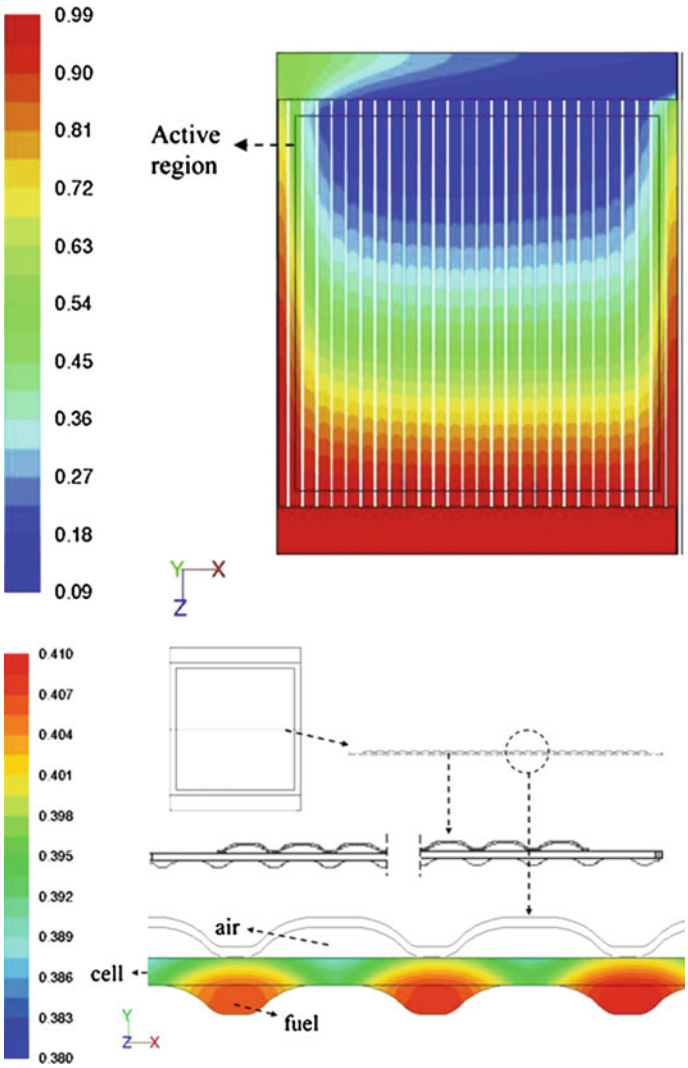

Fig. 8 Mole fraction of H_2 in the anode. *Upper panel top view* of anode surface; *lower panel* SRU cross section (half-cell length). Simulations performed at 973 K, with 5000 A/m^2 average current density and 95 % H_2–5 % H_2O inlet fuel and air on the cathode side. [Reprinted with permission from Qu et al. (2011)]

7 Summary and Conclusions

A SOFC is a complex system consisting of different components, each one composed of peculiar materials in which interconnected physical phenomena occur simultaneously involving gas and solid phases. Modeling an SOFC can be performed following different approaches, depending on the particular component on which the model is focused. This chapter introduced a physically based modeling approach, which entails the macroscopic description of the phenomena.

The equations of mass, energy, momentum, charge transport, and conservation were introduced, and their application in the different domains (i.e., fluid, porous, and solid) was assessed. Common approaches for modeling electrochemistry and heterogeneous chemical reactions were discussed.

Results from the literature were also presented to show multidimensional applications of the physically based modeling approach described. The mathematical models introduced and the examples given show that a universal formulation suitable for solving all SOFC modeling problems does not exist. Indeed, the way in which the description of the interconnected phenomena is established in a model framework strongly depends on the level of approximation desired and on the final objective of the model.

References

Achenbach, E., & Riensche, E. (1994). Methane/steam reforming kinetics for solid oxide fuel cells. *Journal of Power Sources, 52*(2), 283–288.

Ahmed, K., & Foger, K. (2000). Kinetics of internal steam reforming of methane on Ni/YSZ-based anodes for solid oxide fuel cells. *Catalysis Today, 63*(2), 479–487.

Amhalhel, G., & Furmański, P. (1997). Problems of modeling flow and heat transfer in porous media. *Journal of Power Technologies, 85*, 55–88.

Andersson, M., Yuan, J., & Sundén, B. (2010). Review on modeling development for multiscale chemical reactions coupled transport phenomena in solid oxide fuel cells. *Applied Energy, 87* (5), 1461–1476.

Andersson, M., Yuan, J., & Sundén, B. (2012). SOFC modeling considering electrochemical reactions at the active three phase boundaries. *International Journal of Heat and Mass Transfer, 55*(4), 773–788.

Andersson, M., Yuan, J., & Sundén, B. (2013). SOFC modeling considering hydrogen and carbon monoxide as electrochemical reactants. *Journal of Power Sources, 232*, 42–54.

Bagotsky, V. S. (Ed.). (2005). *Fundamentals of electrochemistry* (2nd ed., Vol. 44). New York: John Wiley & Sons.

Bear, J. (1972). *Dynamics of fluids in porous media*. New York: American Elsevier.

Belyaev, V. D., Politova, T. I., Mar'ina, O. A., & Sobyanin, V. A. (1995). Internal steam reforming of methane over Ni-based electrode in solid oxide fuel cells. *Applied Catalysis, A: General, 133*(1), 47–57.

Bertei, A., & Nicolella, C. (2015). Common inconsistencies in modeling gas transport in porous electrodes: The dusty-gas model and the Fick law. *Journal of Power Sources, 279*, 133–137.

Bird, R., Steward, W., & Lightfoot, E. (2006). *Transport phenomena*. Amsterdam: John Wiley & Sons. (Revised 2nd edn).

Brinkman, H. C. (1949a). A calculation of the viscous force exerted by a flowing fluid on a dense swarm of particles. *Applied Scientific Research, 1*(1), 27–34.

Brinkman, H. C. (1949b). On the permeability of media consisting of closely packed porous particles. *Applied Scientific Research, 1*(1), 81–86.

Bruggeman, D. A. G. (1935). Calculation of the various physical constants of heterogeneous substances. Dielectric constants and conductivities of mixtures of isotropic substances. *Annual Physik, 24*, 636–664.

Brus, G., Miyawaki, K., Iwai, H., Saito, M., & Yoshida, H. (2014). Tortuosity of an SOFC anode estimated from saturation currents and a mass transport model in comparison with a real micro-structure. *Solid State Ionics, 265*, 13–21.

Cai, Q., Adjiman, C. S., & Brandon, N. P. (2011). Investigation of the active thickness of solid oxide fuel cell electrodes using a 3D microstructure model. *Electrochimica Acta, 56*(28), 10809–10819.

Carman, P. C. (1956). *Flow of gases through porous media*. Waltham: Academic Press.

Cayan, F. N., Pakalapati, S. R., Elizalde-Blancas, F., & Celik, I. (2009). On modeling multi-component diffusion inside the porous anode of solid oxide fuel cells using Fick's model. *Journal of Power Sources, 192*(2), 467–474.

Chan, S. H., Khor, K. A., & Xia, Z. T. (2001). *Journal of Power Sources, 93*(1), 130–140.

Costamagna, P., Costa, P., & Antonucci, V. (1998). Micro-modelling of solid oxide fuel cell electrodes. *Electrochimica Acta, 43*(3), 375–394.

Costamagna, P., & Honegger, K. (1998). Modeling of solid oxide heat exchanger integrated stacks and simulation at high fuel utilization. *Journal of the Electrochemical Society, 145*(11), 3995–4007.

Costamagna, P., Selimovic, A., Del Borghi, M., & Agnew, G. (2004). Electrochemical model of the integrated planar solid oxide fuel cell (IP-SOFC). *Chemical Engineering Journal, 102*(1), 61–69.

Curtiss, C. F., & Bird, R. B. (1999). Multicomponent diffusion. *Industrial and Engineering Chemistry Research, 38*(7), 2515–2522.

Damm, D. L., & Fedorov, A. G. (2004). Spectral radiative heat transfer analysis of the planar SOFC. In *Proceedings of the ASME IMECE*, Anaheim, CA, November 13–19, 2004. Paper No. IMECE2004-60142.

Damm, D. L., & Fedorov, A. G. (2005). Radiation heat transfer in SOFC materials and components. *Journal of Power Sources, 143*(1), 158–165.

Damm, D. L., & Fedorov, A. G. (2006). Local thermal non-equilibrium effects in porous electrodes of the hydrogen-fueled SOFC. *Journal of Power Sources, 159*(2), 1153–1157.

Désilets, M., Proulx, P., & Soucy, G. (1997). Modeling of multicomponent diffusion in high temperature flows. *International Journal of Heat and Mass Transfer, 40*(18), 4273–4278.

Dicks, A. L., Pointon, K. D., & Siddle, A. (2000). Intrinsic reaction kinetics of methane steam reforming on a nickel/zirconia anode. *Journal of Power Sources, 86*(1), 523–530.

Drescher, I., Lehnert, W., & Meusinger, J. (1998). Structural properties of SOFC anodes and reactivity. *Electrochimica Acta, 43*(19), 3059–3068.

Elizalde-Blancas, F., Celik, I. B., Rangel-Hernandez, V., Hernandez-Guerrero, A., & Riesco-Avila, J. M. (2013). Numerical modeling of SOFCs operating on biogas from biodigesters. *International Journal of Hydrogen Energy, 38*(1), 377–384.

Ferguson, J. R., Fiard, J. M., & Herbin, R. (1996). Three-dimensional numerical simulation for various geometries of solid oxide fuel cells. *Journal of Power Sources, 58*(2), 109–122.

Ferrero, D., Lanzini, A., Leone, P., & Santarelli, M. (2015). Reversible operation of solid oxide cells under electrolysis and fuel cell modes: Experimental study and model validation. *Chemical Engineering Journal, 274*, 143–155.

Froment, G. F., Bischoff, K. B., & De Wilde, J. (1990). *Chemical reactor analysis and design* (Vol. 2). New York: Wiley.

Fuller, E. N., Schettler, P. D., & Giddings, J. C. (1966). New method for prediction of binary gas-phase diffusion coefficients. *Industrial and Engineering Chemistry, 58*(5), 18–27.

Funahashi, Y., Shimamori, T., Suzuki, T., Fujishiro, Y., & Awano, M. (2007). Fabrication and characterization of components for cube shaped micro tubular SOFC bundle. *Journal of Power Sources, 163*(2), 731–736.

García-Camprubí, M. (2011). *Multiphysics models for the simulation of solid oxide fuel cells*. (Ph. D., dissertation). University of Zaragoza.

García-Camprubí, M., Sánchez-Insa, A., & Fueyo, N. (2010). Multimodal mass transfer in solid-oxide fuel-cells. *Chemical Engineering Science, 65*(5), 1668–1677.

Geisler, H., Kromp, A., Weber, A., & Ivers-Tiffée, E. (2014). Stationary FEM model for performance evaluation of planar solid oxide fuel cells connected by metal interconnectors I. Model framework and validation. *Journal of the Electrochemical Society, 161*(6), F778–F788.

Goldin, G. M., Zhu, H., Kee, R. J., Bierschenk, D., & Barnett, S. A. (2009). Multidimensional flow, thermal, and chemical behavior in solid-oxide fuel cell button cells. *Journal of Power Sources, 187*(1), 123–135.

Goodwin, D. G., Zhu, H., Colclasure, A. M., & Kee, R. J. (2009). Modeling electrochemical oxidation of hydrogen on Ni–YSZ pattern anodes. *Journal of the Electrochemical Society, 156* (9), B1004–B1021.

Greene, E. S., Chiu, W. K., & Medeiros, M. G. (2006). Mass transfer in graded microstructure solid oxide fuel cell electrodes. *Journal of Power Sources, 161*(1), 225–231.

Grew, K. N., & Chiu, W. K. (2012). A review of modeling and simulation techniques across the length scales for the solid oxide fuel cell. *Journal of Power Sources, 199*, 1–13.

Gupta, G. K., Hecht, E. S., Zhu, H., Dean, A. M., & Kee, R. J. (2006). Gas-phase reactions of methane and natural-gas with air and steam in non-catalytic regions of a solid-oxide fuel cell. *Journal of Power Sources, 156*(2), 434–447.

Haberman, B. A., & Young, J. B. (2004). Three-dimensional simulation of chemically reacting gas flows in the porous support structure of an integrated-planar solid oxide fuel cell. *International Journal of Heat and Mass Transfer, 47*(17), 3617–3629.

Hajimolana, S. A., Hussain, M. A., Daud, W. A. W., Soroush, M., & Shamiri, A. (2011). Mathematical modeling of solid oxide fuel cells: A review. *Renewable and Sustainable Energy Reviews, 15*(4), 1893–1917.

Hanna, J., Lee, W. Y., Shi, Y., & Ghoniem, A. F. (2014). Fundamentals of electro-and thermochemistry in the anode of solid-oxide fuel cells with hydrocarbon and syngas fuels. *Progress in Energy and Combustion Science, 40*, 74–111.

Hao, Y., & Goodwin, D. G. (2008). Numerical study of heterogeneous reactions in an SOFC anode with oxygen addition. *Journal of the Electrochemical Society, 155*(7), B666–B674.

He, W., Lu, W., & Dickerson, J. H. (2014a). *Chapter 2: Gas diffusion in porous media gas transport in solid oxide fuel cells* (1st ed., pp. 9–17). New York: Springer.

He, W., Lu, W., & Dickerson, J. H. (2014b). *Gas transport in solid oxide fuel cells*. New York: Springer.

Hecht, E. S., Gupta, G. K., Zhu, H., Dean, A. M., Kee, R. J., Maier, L., et al. (2005). Methane reforming kinetics within a Ni–YSZ SOFC anode support. *Applied Catalysis, A: General, 295*(1), 40–51.

Hernández-Pacheco, E., Singh, D., Hutton, P. N., Patel, N., & Mann, M. D. (2004). A macro-level model for determining the performance characteristics of solid oxide fuel cells. *Journal of Power Sources, 138*(1), 174–186.

Hirschfelder, J. O., Curtiss, C. F., Bird, R. B., & Mayer, M. G. (1954). *Molecular theory of gases and liquids* (Vol. 26, p. 10). New York: Wiley.

Ho, T. X., Kosinski, P., Hoffmann, A. C., & Vik, A. (2008). Numerical modeling of solid oxide fuel cells. *Chemical Engineering Science, 63*(21), 5356–5365.

Ho, T. X., Kosinski, P., Hoffmann, A. C., & Vik, A. (2009). Modeling of transport, chemical and electrochemical phenomena in a cathode-supported SOFC. *Chemical Engineering Science, 64*(12), 3000–3009.

Hofmann, P., Panopoulos, K. D., Fryda, L. E., & Kakaras, E. (2009). Comparison between two methane reforming models applied to a quasi-two-dimensional planar solid oxide fuel cell model. *Energy, 34*(12), 2151–2157.

Hosoi, T., Yonekura, T., Sunada, K., & Sasaki, K. (2015). Exchange current density of SOFC electrodes: Theoretical relations and partial pressure dependencies rate-determined by electrochemical reactions. *Journal of the Electrochemical Society, 162*(1), F136–F152.

Hou, K., & Hughes, R. (2001). The kinetics of methane steam reforming over a Ni/α-Al_2O catalyst. *Chemical Engineering Journal, 82*(1), 311–328.

Hsu, C. T., & Cheng, P. (1990). Thermal dispersion in a porous medium. *International Journal of Heat and Mass Transfer, 33*(8), 1587–1597.

Hussain, M. M., Li, X., & Dincer, I. (2005). Multi-component mathematical model of solid oxide fuel cell anode. *International Journal of Energy Research, 29*(12), 1083–1101.

Iwai, H., Shikazono, N., Matsui, T., Teshima, H., Kishimoto, M., Kishida, R., et al. (2010). Quantification of SOFC anode microstructure based on dual beam FIB-SEM technique. *Journal of Power Sources, 195*(4), 955–961.

Janardhanan, V. M., & Deutschmann, O. (2006). CFD analysis of a solid oxide fuel cell with internal reforming: Coupled interactions of transport, heterogeneous catalysis and electrochemical processes. *Journal of Power Sources, 162*(2), 1192–1202.

Janardhanan, V. M., & Deutschmann, O. (2007). Numerical study of mass and heat transport in solid-oxide fuel cells running on humidified methane. *Chemical Engineering Science, 62*(18), 5473–5486.

Janardhanan, V. M., Heuveline, V., & Deutschmann, O. (2008). Three-phase boundary length in solid-oxide fuel cells: A mathematical model. *Journal of Power Sources, 178*(1), 368–372.

Jiang, Y., & Virkar, A. V. (2003). Fuel composition and diluent effect on gas transport and performance of anode-supported SOFCs. *Journal of the Electrochemical Society, 150*(7), A942–A951.

Joos, J., Carraro, T., Weber, A., & Ivers-Tiffée, E. (2011). Reconstruction of porous electrodes by FIB/SEM for detailed microstructure modeling. *Journal of Power Sources, 196*(17), 7302–7307.

Jung, H. Y., Kim, W. S., Choi, S. H., Kim, H. C., Kim, J., Lee, H. W., et al. (2006). Effect of cathode current-collecting layer on unit-cell performance of anode-supported solid oxide fuel cells. *Journal of Power Sources, 155*(2), 145–151.

Kast, W., & Hohenthanner, C. R. (2000). Mass transfer within the gas-phase of porous media. *International Journal of Heat and Mass Transfer, 43*(5), 807–823.

Kerkhof, P. J. (1996). A modified Maxwell–Stefan model for transport through inert membranes: The binary friction model. *The Chemical Engineering Journal and the Biochemical Engineering Journal, 64*(3), 319–343.

Kim, J. H., Liu, W. K., & Lee, C. (2009). Multi-scale solid oxide fuel cell materials modeling. *Computational Mechanics, 44*(5), 683–703.

Kishimoto, M., Iwai, H., Saito, M., & Yoshida, H. (2011). Quantitative evaluation of solid oxide fuel cell porous anode microstructure based on focused ion beam and scanning electron microscope technique and prediction of anode overpotentials. *Journal of Power Sources, 196*(10), 4555–4563.

Klein, J. M., Bultel, Y., Georges, S., & Pons, M. (2007). Modeling of a SOFC fuelled by methane: From direct internal reforming to gradual internal reforming. *Chemical Engineering Science, 62*(6), 1636–1649.

Kong, W., Zhu, H., Fei, Z., & Lin, Z. (2012). A modified dusty gas model in the form of a Fick's model for the prediction of multicomponent mass transport in a solid oxide fuel cell anode. *Journal of Power Sources, 206*, 171–178.

Krishna, R., & Wesselingh, J. A. (1997). The Maxwell–Stefan approach to mass transfer. *Chemical Engineering Science, 52*(6), 861–911.

Lage, J. L. (1993). Natural convection within a porous medium cavity: Predicting tools for flow regime and heat transfer. *International Communications in Heat and Mass Transfer, 20*(4), 501–513.

Lanzini, A., Leone, P., & Asinari, P. (2009). Microstructural characterization of solid oxide fuel cell electrodes by image analysis technique. *Journal of Power Sources, 194*(1), 408–422.

Laurencin, J., Kane, D., Delette, G., Deseure, J., & Lefebvre-Joud, F. (2011). Modelling of solid oxide steam electrolyser: Impact of the operating conditions on hydrogen production. *Journal of Power Sources, 196*(4), 2080–2093.

Lee, A. L., Zabransky, R. F., & Huber, W. J. (1990). Internal reforming development for solid oxide fuel cells. *Industrial and Engineering Chemistry Research, 29*(5), 766–773.

Lee, K. T., Vito, N. J., & Wachsman, E. D. (2013). Comprehensive quantification of Ni–$Gd_{0.1}Ce_{0.9}O_{1.95}$ anode functional layer microstructures by three-dimensional reconstruction using a FIB/SEM dual beam system. *Journal of Power Sources, 228*, 220–228.

Lehnert, W., Meusinger, J., & Thom, F. (2000). Modelling of gas transport phenomena in SOFC anodes. *Journal of Power Sources, 87*(1), 57–63.

Leonide, A. (2010). *SOFC modelling and parameter identification by means of impedance spectroscopy* (Ph.D. dissertation). Karlsruher Institut für Technologie.

Li, Y., Gemmen, R., & Liu, X. (2010). Oxygen reduction and transportation mechanisms in solid oxide fuel cell cathodes. *Journal of Power Sources, 195*(11), 3345–3358.

Mason, E. A., & Malinauskas, A. P. (1983). *Gas transport in porous media: The dusty-gas model* (pp. 1–202). New York: Elsevier.

Matsuzaki, K., Shikazono, N., & Kasagi, N. (2011). Three-dimensional numerical analysis of mixed ionic and electronic conducting cathode reconstructed by focused ion beam scanning electron microscope. *Journal of Power Sources, 196*(6), 3073–3082.

Menon, V., Janardhanan, V. M., Tischer, S., & Deutschmann, O. (2013). Internal multi-physics phenomena of SOFC with direct internal reforming. *ECS Transactions, 57*(1), 2475–2484.

Modest, M. F. (2013). *Radiative heat transfer* (3rd ed.). New York: Academic Press.

Moon, H., Kim, S. D., Park, E. W., Hyun, S. H., & Kim, H. S. (2008). Characteristics of SOFC single cells with anode active layer via tape casting and co-firing. *International Journal of Hydrogen Energy, 33*(11), 2826–2833.

Murthy, S., & Fedorov, A. G. (2003). Radiation heat transfer analysis of the monolith type solid oxide fuel cell. *Journal of Power Sources, 124*(2), 453–458.

Nagel, F. P., Schildhauer, T. J., Biollaz, S. M., & Stucki, S. (2008). Charge, mass and heat transfer interactions in solid oxide fuel cells operated with different fuel gases—a sensitivity analysis. *Journal of Power Sources, 184*(1), 129–142.

Nam, J. H., & Jeon, D. H. (2006). A comprehensive micro-scale model for transport and reaction in intermediate temperature solid oxide fuel cells. *Electrochimica Acta, 51*(17), 3446–3460.

Ni, M. (2009). Computational fluid dynamics modeling of a solid oxide electrolyzer cell for hydrogen production. *International Journal of Hydrogen Energy, 34*(18), 7795–7806.

Ni, M. (2013). Modeling and parametric simulations of solid oxide fuel cells with methane carbon dioxide reforming. *Energy Conversion and Management, 70*, 116–129.

Ni, M., Leung, M. K., & Leung, D. Y. (2007). Parametric study of solid oxide fuel cell performance. *Energy Conversion and Management, 48*(5), 1525–1535.

Nield, D. A., & Bejan, A. (2006). *Chapter 1: Mechanics of fluid flow through a porous medium—convection in porous media* (3rd ed., pp. 1–26). New York: Springer.

Noren, D. A., & Hoffman, M. A. (2005). Clarifying the Butler–Volmer equation and related approximations for calculating activation losses in solid oxide fuel cell models. *Journal of Power Sources, 152*, 175–181.

Novaresio, V., García-Camprubí, M., Izquierdo, S., Asinari, P., & Fueyo, N. (2012). An open-source library for the numerical modeling of mass-transfer in solid oxide fuel cells. *Computer Physics Communications, 183*(1), 125–146.

Park, E. W., Moon, H., Park, M. S., & Hyun, S. H. (2009). Fabrication and characterization of Cu–Ni–YSZ SOFC anodes for direct use of methane via Cu-electroplating. *International Journal of Hydrogen Energy, 34*(13), 5537–5545.

Poling, B. E., Prausnitz, J. M., & O'connell, J. P. (2001). *The properties of gases and liquids* (Vol. 5, pp. 11.5–11.9). New York: McGraw-Hill.

Pollard, W. G., & Present, R. D. (1948). On gaseous self-diffusion in long capillary tubes. *Physical Review, 73*(7), 762.

Qu, Z., Aravind, P. V., Boksteen, S. Z., Dekker, N. J. J., Janssen, A. H. H., Woudstra, N., et al. (2011). Three-dimensional computational fluid dynamics modeling of anode-supported planar SOFC. *International Journal of Hydrogen Energy, 36*(16), 10209–10220.

Ramshaw, J. D. (1990). Self-consistent effective binary diffusion in multicomponent gas mixtures. *Journal of Non-Equilibrium Thermodynamics, 15*(3), 295–300.

Sanchez, D., Chacartegui, R., Munoz, A., & Sanchez, T. (2008). On the effect of methane internal reforming modelling in solid oxide fuel cells. *International Journal of Hydrogen Energy, 33*(7), 1834–1844.

Sánchez, D., Munoz, A., & Sánchez, T. (2007). An assessment on convective and radiative heat transfer modelling in tubular solid oxide fuel cells. *Journal of Power Sources, 169*(1), 25–34.

Santarelli, M., Quesito, F., Novaresio, V., Guerra, C., Lanzini, A., & Beretta, D. (2013). Direct reforming of biogas on Ni-based SOFC anodes: Modelling of heterogeneous reactions and validation with experiments. *Journal of Power Sources, 242*, 405–414.

Shi, Y., Cai, N., & Li, C. (2007). Numerical modeling of an anode-supported SOFC button cell considering anodic surface diffusion. *Journal of Power Sources, 164*(2), 639–648.

Shi, Y., Li, C., & Cai, N. (2011). Experimental characterization and mechanistic modeling of carbon monoxide fueled solid oxide fuel cell. *Journal of Power Sources, 196*(13), 5526–5537.

Suwanwarangkul, R., Croiset, E., Fowler, M. W., Douglas, P. L., Entchev, E., & Douglas, M. A. (2003). Performance comparison of Fick's, dusty-gas and Stefan–Maxwell models to predict the concentration overpotential of a SOFC anode. *Journal of Power Sources, 122*(1), 9–18.

Tseronis, K., Kookos, I. K., & Theodoropoulos, C. (2008). Modelling mass transport in solid oxide fuel cell anodes: A case for a multidimensional dusty gas-based model. *Chemical Engineering Science, 63*(23), 5626–5638.

Veldsink, J. W., Van Damme, R. M. J., Versteeg, G. F., & Van Swaaij, W. P. M. (1995). The use of the dusty-gas model for the description of mass transport with chemical reaction in porous media. *The Chemical Engineering Journal and the Biochemical Engineering Journal, 57*(2), 115–125.

Walters, K. M., Dean, A. M., Zhu, H., & Kee, R. J. (2003). Homogeneous kinetics and equilibrium predictions of coking propensity in the anode channels of direct oxidation solid-oxide fuel cells using dry natural gas. *Journal of Power Sources, 123*(2), 182–189.

Wang, K., Hissel, D., Péra, M. C., Steiner, N., Marra, D., Sorrentino, M., et al. (2011a). A review on solid oxide fuel cell models. *International Journal of Hydrogen Energy, 36*(12), 7212–7228.

Wang, S., Worek, W. M., & Minkowycz, W. J. (2012). Performance comparison of the mass transfer models with internal reforming for solid oxide fuel cell anodes. *International Journal of Heat and Mass Transfer, 55*(15), 3933–3945.

Wang, Y., Weng, S., & Weng, Y. (2011b). Numerical investigation of the chemical and electrochemical characteristics of planar solid oxide fuel cell with direct internal reforming. *Frontiers in Energy, 5*(2), 195–206.

Webb, S. W., & Pruess, K. (2003). The use of Fick's law for modeling trace gas diffusion in porous media. *Transport in Porous Media, 51*(3), 327–341.

Welty, J. R., Wicks, C. E., Rorrer, G., & Wilson, R. E. (2001). *Fundamentals of momentum, heat, and mass transfer* (4th ed.). New York: John Wiley & Sons.

Wilke, C. R. (1950a). A viscosity equation for gas mixtures. *The Journal of Chemical Physics, 18*(4), 517–519.

Wilke, C. R. (1950b). Diffusional properties of multicomponent gases. *Chemical Engineering Progress, 46*, 95–104.

Wilson, J. R., Cronin, J. S., & Barnett, S. A. (2011). Linking the microstructure, performance and durability of Ni-yttria-stabilized zirconia solid oxide fuel cell anodes using three-dimensional focused ion beam–scanning electron microscopy imaging. *Scripta Materialia, 65*(2), 67–72.

Wu, W., Wang, G. L., Guan, W. B., Zhen, Y. F., & Wang, W. G. (2013). Effect of contact method between interconnects and electrodes on area specific resistance in planar solid oxide fuel cells. *Fuel Cells, 13*(5), 743–750.

Xu, J., & Froment, G. F. (1989). Methane steam reforming, methanation and water–gas shift: I. Intrinsic kinetics. *AIChE Journal, 35*(1), 88–96.

Yakabe, H., Hishinuma, M., Uratani, M., Matsuzaki, Y., & Yasuda, I. (2000). Evaluation and modeling of performance of anode-supported solid oxide fuel cell. *Journal of Power Sources, 86*(1), 423–431.

Yakabe, H., Ogiwara, T., Hishinuma, M., & Yasuda, I. (2001). 3-D model calculation for planar SOFC. *Journal of Power Sources, 102*(1), 144–154.

Zheng, K., Sun, Q., & Ni, M. (2013). Local non-equilibrium thermal effects in solid oxide fuel cells with various fuels. *Energy Technology, 1*(1), 35–41.

Zhu, H., & Kee, R. J. (2003). A general mathematical model for analyzing the performance of fuel-cell membrane-electrode assemblies. *Journal of Power Sources, 117*(1), 61–74.

Zhu, H., & Kee, R. J. (2008). Modeling distributed charge-transfer processes in SOFC membrane electrode assemblies. *Journal of the Electrochemical Society, 155*(7), B715–B729.

Zhu, H., Kee, R. J., Janardhanan, V. M., Deutschmann, O., & Goodwin, D. G. (2005). Modeling elementary heterogeneous chemistry and electrochemistry in solid-oxide fuel cells. *Journal of the Electrochemical Society, 152*(12), A2427–A2440.